*University of Alberta*
*Printing Department*

THE UNIVERSITY OF ALBERTA

# A COINCIDENCE GAMMA-RAY SPECTROMETER WITH APPLICATIONS

A THESIS

SUBMITTED TO THE FACULTY OF GRADUATE STUDIES

IN PARTIAL FULFILMENT OF THE REQUIREMENTS FOR THE DEGREE

OF MASTER OF SCIENCE

DEPARTMENT OF PHYSICS

by

RICHARD GRAHAM MILLER

EDMONTON, ALBERTA

SEPTEMBER, 1961

UNIVERSITY OF ALBERTA

FACULTY OF GRADUATE STUDIES

The undersigned certify that they have read, and recommend to the Faculty of Graduate Studies for acceptance, a thesis entitled A COINCIDENCE GAMMA-RAY SPECTROMETER WITH APPLICATIONS, submitted by Richard Graham Miller in partial fulfilment of the requirements for the degree of Master of Science.

Professor

Professor

Professor

Professor

Date Sept 7 1961

ABSTRACT

A sum-coincidence gamma-ray spectrometer, developed by Hoogenboom, has been further developed and used to measure the angular correlation of the gamma rays in the $Co^{60}(\beta^-,\gamma\gamma')$ cascade and to measure the yield of cascading gamma rays from the 1.74, 2.15 and 3.58 Mev. levels of $B^{10}$ formed in the reaction $Be^9(d,n)B^{10}$. The yield curves obtained do not show the existence of a resonance in the yield cross-section around 1 Mev., as has been reported. Graphs of the efficiency and resolution of a 4" NaI(Tl) collimated crystal are presented. A discussion of the effects of escaping coincident Compton gamma rays on the background of a Hoogenboom Spectrometer is given.

ABSTRACT

A sum-coincidence gamma-ray spectrometer, developed by Hoogenboom, has been further developed and used to measure the angular correlation of the gamma rays in the $Co^{60}(\beta^-,\gamma\gamma')$ cascade and to measure the yield of cascading gamma rays from the 1.74, 2.15 and 3.58 Mev. levels of $B^{10}$ formed in the reaction $Be^9(d,n)B^{10}$. The yield curves obtained do not show the existence of a resonance in the yield cross-section around 1 Mev., as has been reported. Graphs of the efficiency and resolution of a 4" NaI(Tl) collimated crystal are presented. A discussion of the effects of escaping coincident Compton gamma rays on the background of a Hoogenboom Spectrometer is given.

ACKNOWLEDGEMENTS

I find this acknowledgement very difficult to write since more than a dozen people have helped to make the completion of this project possible.

First the Professors of the Van de Graaff Group, Doctors G. C. Neilson, W. K. Dawson and J. T. Sample. I would particularly like to thank my supervisor, Dr. G. C. Neilson, for suggesting this project and for generous help at all stages.

Then the technicians: L. Holm, who helped build the electronics; C. Green, who made the collimators and source holders; and J. B. Elliott, who helped with just about everything.

Lastly, I would like to thank all the students of the group, in particular P. J. Riley and W. G. Davies for help in running the Van de Graaff, and J. F. Easton for efficiency calculations performed on the computer.

TABLE OF CONTENTS

LIST OF FIGURES

List of Figures

# INTRODUCTION

Nuclear spectroscopy may be said to have started in 1932 when Cockroft and Walton developed the first machine for accelerating charged particles to produce nuclear reactions. Since that time, a great deal of empirical information has been obtained about the structure of nuclei and some success has been had in fitting this knowledge into a theoretical framework. In fact, the shell and collective models of nuclear structure, when taken together, can predict the spin, parity, and isotopic spin of the ground states of almost all nuclei and can be applied with considerable success to predict the properties of excited states. Unquantized parameters, such as magnetic dipole and electric quadrupole moments can also be predicted with some success. However, a really complete theory of nuclear structure is still lacking. There are some people who say that such a theory will never be found; that the problem is too difficult for an exact solution. Be that as it may, it is certain that new attempts will be made.

One of the most sensitive tests of any theory developed is whether or not it can predict allowed gamma-ray

transitions and their relative intensities. Thus the study of gamma rays is an important field of nuclear investigation. A perhaps even more important aspect of gamma-ray spectroscopy is that the measurement of angular distributions and correlations of gamma rays produced in nuclear reactions often yields important information about the nuclear levels involved, such as their angular momentum and parity.

Gamma-ray spectroscopy has been revolutionized by the recent development of scintillation detection techniques. However, a scintillation crystal gamma-ray detector has two serious drawbacks: A large "background" count is produced by events in which only part of the energy of the incident gamma ray is detected and the width of the full-energy gamma-ray peak is greatly broadened over its natural width as defined by the uncertainty principle.

## SECTION 1. SIMPLE THEORY OF ANGULAR CORRELATIONS

Consider an isolated nucleus in an excited state. The probability of the emission of radiation in a given direction depends on the angle between the emission direction and the nuclear spin. Normally one deals with a large assembly of nuclei with randomly oriented spins so that the angular distribution of the resulting radiation is isotropic. To see an anisotropic distribution, one must effectively align the nuclear spins. This can be accomplished either by an actual alignment of the nuclei, which is rather difficult to do, or by observing preferentially the radiation produced by those nuclei with certain spin orientations, which can often be done quite easily and is the method discussed here. In particular, an anisotropic distribution can be observed whenever the nuclei de-excite by emitting two radiations in cascade, except when one of the radiations is a particle with zero angular momentum or one of the nuclear levels involved has a spin of 0 or 1/2. Here, only de-excitation by the cascade emission of gamma rays will be discussed.

Consider the cascade scheme of Figure 1-1. $j_1$, $j$ and $j_2$ are the total angular momenta and $m_1$, $m$ and $m_2$

a particular set of magnetic substates of the nuclear levels involved. $L_1, L_2$ and $M_1, M_2$ are the multipolarities and magnetic quantum numbers respectively of $\gamma_1$ and $\gamma_2$. If $\gamma_1$ is observed in only one direction, those particular nuclei which emitted $\gamma_1$ will have a non-uniform spin distribution so that $\gamma_2$ will possess a definite angular correlation with respect to the emission direction of $\gamma_1$. This correlation, $W(\theta)$, can be observed by measuring the number of coincidences between $\gamma_1$ and $\gamma_2$ in two different counters as a function of the angle between them.

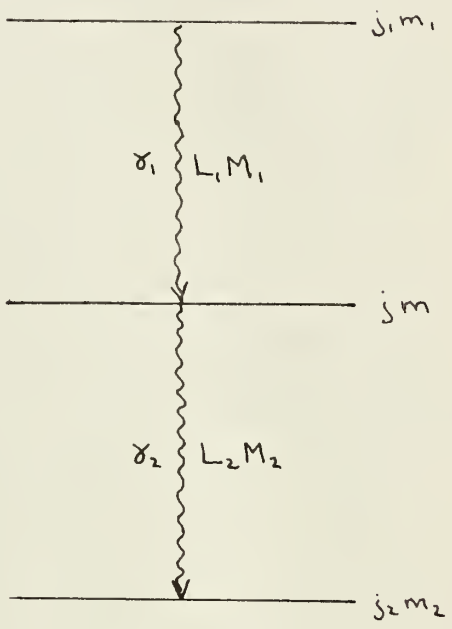


Figure 1-1

For the sake of simplicity, some special assumptions will now be made about the nature of the cascade. First, it is assumed that $\gamma_1$ and $\gamma_2$ are pure multipole transitions of multipolarity $L_1$ and $L_2$ respectively. Secondly, it is assumed that the intermediate state, $j$, is unperturbed by any extra-nuclear forces. This is equivalent to assuming that the life time of the intermediate

state is short compared to the time required for the extra-nuclear forces present to appreciably affect it, a condition which is often true, especially for transitions of low multipole order.

Consider two particular components in the transition $j_1 \to j \to j_2$ e.g. those components in which the nucleus first jumps from the sub-state of $j_1$ with projection quantum number $m_1$ to the sub-state of $j$ with projection quantum number $m$ emitting a gamma ray with projection number $M_1 = m_1 - m$, and the following jump from $jm$ to $j_2 m_2$ yielding a gamma ray with projection number $M_2 = m - m_2$. Let $N(m_1), N(m)$ and $P(m_1 m), P(m m_2)$ represent the populations (assumed constant) of the $m_1$ and $m$ levels, and the transition probabilities from $m_1$ to $m$ and $m$ to $m_2$ respectively. Furthermore let $T_{L_1}^{M_1}(\Theta_1)$ and $T_{L_2}^{M_2}(\Theta_2)$ represent the angular distributions of the two components about the particular quantization axis chosen. Thus, with $\Theta_1$ being the angle between the direction of emission of $\gamma_1$ and the quantization axis, $T_{L_1}^{M_1}(\Theta_1)$ is the probability of finding the $M_1$ component of $\gamma_1$ in the solid angle $d\Omega$ defined by the direction $\Theta_1$. The $T_L^M$ are the "tensor parameters" of the radiation and depend only on the properties of the radiation itself. At this point, the problem can be greatly simplified by

choosing the z-axis (the quantization axis) in a particular direction, the direction of $\gamma_1$ . Then $\Theta_1 = 0$ and $\Theta_2 = \Theta$ so that $W(\Theta)$ is merely the distribution of $\gamma_2$ about the z-axis. Considering the $m$ to $m_2$ component only, we see that the angular correlation is given by the population of the sub-state $m$ times its probability of decay to $m_2$ times the angular distribution of the emitted radiation, i.e.

$$W_{m \to m_2}(\Theta) = N(m)\, P(m m_2)\, T_{L_2}^{m-m_2}(\Theta) .$$

The observed angular correlation is found by summing over all possible components. Thus

$$W(\Theta) = \sum_{m m_2} N(m)\, P(m m_2)\, T_{L_2}^{m-m_2}(\Theta) \quad (1)$$

$N(m)$ is determined by the properties of the first transition. Using the same reasoning as above, it is given by

$$N(m) = \sum_{m_1} N(m_1)\, P(m_1 m)\, T_{L_1}^{m_1-m}(\Theta=0) . \quad (2)$$

Combining (1) and (2)

$$W(\Theta) = \sum_{m_1 m m_2} N(m_1)\, P(m_1 m)\, P(m\, m_2)\, T_{L_1}^{m_1-m}(0)\, T_{L_2}^{m-m_2}(\Theta) . \quad (3)$$

This combination involves an additional assumption; that the decay $m \to m_2$ is independent of the $m_1$ sub-state from which $m$ is formed. For proof, see Ro 57.

Our special choice of z-axis allows a further simplification. Since the projection quantum number of gamma radiation can only take on the two values $\pm 1$ along its own propagation direction (again see Ro 57 for proof), it follows that $M_1 = \pm 1$ so that

$$W(\Theta) = \sum_{m_1 m_2} N(m_1)\, P(m_1, m_1 \pm 1)\, P(m_1 \pm 1\, m_2)\, T_{L_1}^{\mp 1}(0)\, T_{L_2}^{m_1-m_2 \pm 1}(\Theta) . \quad (4)$$

It can be shown that the absolute transition probability between any two levels $j m$, $j' m'$ for a particular multipole radiation component $L M$ can be written as the product of a nuclear factor and a geometrical factor (Wigner-Eckart Theorem, see Ro 57). The nuclear factor ("reduced matrix element") contains all the specifically nuclear properties of the transition and is constant for a given $j$ to $j'$ transition, independent of the particular sub-states involved, if there is no multipole mixing in the transition. The geometrical factor contains all the $m m'$ dependence (therefore all the angular dependence) and is proportional to the transition probability. The value of this geometrical factor can be obtained by the following "plausibility argument."

Consider a state $j m$ which jumps to a state $j' m'$ by emission of a gamma ray $L M$ under the action of an operator $Q_L$. The operator which induces the transition depends only on the multipolarity of the gamma ray; the effect which it produces depends on the angular momenta of the levels involved but not on the projection numbers $m, m'$ and $M$ which merely describe the geometrical configuration of the system. From perturbation theory,

$$P(mm') \sim |\langle f | Q_L | i \rangle|^2$$

$$\sim |(\psi_{j'm'} \psi_{LM}, Q_L \psi_{jm})|^2. \qquad (5)$$

$\psi_{j'm'}$, $\psi_{jm}$ and $\psi_{LM}$ are the wave functions of the two states and emitted gamma ray. Now write $\psi_{jm} = \varphi_j \eta_{jm}$ etc., where the $\eta_{jm}$ are orthonormal functions related to the spherical harmonics and contain all the invariance properties of the system under rotation and reflection; and the $\varphi_j$ are functions which contain all the intrinsic properties of the system. Since the operator $Q_L$ depends only on the intrinsic properties, the integral in ⑤ separates and we can write

$$P(mm') \sim |(\varphi_{j'} \varphi_L, Q_L \varphi_j)(\eta_{j'm'} \eta_{LM}, \eta_{jm})|^2 . \quad ⑥$$

The first integral is the reduced matrix element $(j' \| Q_L \| j)$. The second integral can be evaluated by making use of the definition of the Clebsch-Gordon (C) coefficients (see Ro 57). Thus

$$\eta_{j'm'} \eta_{LM} = \sum_{j^*} (j' L j^* | m' M m) \eta_{j^* m} . \qquad (m = m' + M)$$

Substituting this in ⑥ and using the orthonormality of the $\eta_{jm}$'s and the reality of the C coefficients, we get

$$P(mm') \sim |(j' \| Q_L \| j)|^2 (j' L j | m' M m)^2 .$$

Since the reduced matrix element is the same for all the transitions involved, it can be divided out as a normalization factor so that

$$P(mm') \sim (j' L j | m' M m)^2 . \quad ⑦$$

(It is here that the simplification introduced by assuming $\gamma_1$ and $\gamma_2$ to be of pure multipole order becomes apparent. If they were not, equation ④ would have to contain a correctly weighted summation over the allowed values of $L_1$ and $L_2$ and the reduced matrix elements could not be divided out. This would indeed be unfortunate because they are largely unknown.)

Making use of ⑦ in ④ , the correlation function finally takes the form

$$W(\theta) \sim \sum_{m_1 m_2} N(m_1) (j L_1 j_1 | m_1 \pm 1 \; M \; m_1)^2 (j_2 L_2 j | m_2 M_2 m_1 \pm 1)^2 \times T_{L_1}^{\pm 1}(0) \, T_{L_2}^{m_1 - m_2 \pm 1}(\theta) . \qquad ⑧$$

The only unknown factor in this expression is $N(m_1)$. The simplest case is that with $N(m_1)$ constant, the case for a gamma-ray source whose spins are randomly oriented such as in the radioactive decay $Co^{60}(\beta^-, \gamma\gamma')Ni^{60}$. The anisotropy, $A$ , defined as $A = [W(180°) - W(90°)] / W(90°)$, has a value of 0.167 for this reaction. Since this anisotropy is large enough to be easily observed and since a $Co^{60}$ source is easily prepared, the $Ni^{60}$ $\gamma$-$\gamma'$ correlation is taken as a standard reaction for the testing of equipment.

However, in general $N(m_1)$ is not a constant independent of $m_1$ . Suppose one is looking at cascading gamma rays produced by bombardment of a target with charged

particles. Then the initial state of the cascade is definitely not populated isotropically unless it has an angular momentum of 0 or 1/2 , or is formed by the capture of an s wave particle. In general, one is now concerned with a triple correlation since the beam direction, as well as the direction of the two gamma rays, enters the correlation function. To use equation ⑧ , one would have to know $N(m_1)$ expressed for the already chosen quantization axis - the direction of $\gamma_1$ . Unless the detector is located at $0^\circ$, $N(m_1)$ will not possess symmetry about this direction and will be very difficult to evaluate.

A different approach is necessary. This approach, based on group theory and Racah algebra, leads to a simpler result than ⑧ for the double correlation as well (see Bi 53, Fr 55 and Ro 57). The basic idea is as follows: The special choice of quantization axis along the direction of $\gamma_1$ produced an apparent large simplification but actually it destroyed the inherent symmetry of the problem. The two gamma rays of the cascade are of an identical nature whereas the derivation of ⑧ singled out the second one for special attention. A more natural method is to describe each gamma ray in its own co-ordinate system with z-axis chosen along the direction

of emission of each and then to relate the two co-ordinate systems to an arbitrary z-axis by means of the transformation properties of the two radiations. In the case of a triple correlation, this arbitrary axis can be chosen as the beam direction.

When the general theory is applied to a double correlation, one is lead to the expression

$$W(\theta) = \sum_{\substack{n=0 \\ (n \text{ integral})}}^{n_{max}} a_{2n} P_{2n}(\cos\theta) \qquad (9)$$

where $n_{max}$ is the smallest of $(2j, 2L_1, 2L_2)$ . This condition usually gives $n_{max}=1$ or 2 . The coefficients $a_{2n}$ are functions of the angular momenta (but not the parity) of the levels involved and are listed for all cases of interest by Bi 53. The experimental procedure is to measure the correlation, express it in the form of (9) , and compare the coefficients $a_{2n}$ so obtained with the theoretical coefficients (corrected for the geometry and efficiency of the detection system - see section 5-1) for the different possible sets of $j$ values.

For a triple correlation, the expression obtained (Li 61) is

$$W(\theta_1, \theta_2, \varphi) = \sum_{k_1 k_2 \varkappa} a^{\varkappa}_{k_1 k_2} P^{\varkappa}_{k_1}(\cos\theta_1) P^{\varkappa}_{k_2}(\cos\theta_2) \cos\varkappa\varphi \qquad (10)$$

where $\Theta_1$ and $\Theta_2$ are the polar angles of the two gamma rays with respect to the beam direction and $\Phi$ is the relative azimuthal angle between the gamma rays (see Figure 1-2). If the gamma rays have a multipolarity no greater than four and the spins and parities of the levels involved are unique, then $k_1$ and $k_2$ are even and less than or equal to four and $\kappa$ takes on all integral values from zero to the smaller of $k_1$ and $k_2$. In this case, the series (10) has 19 terms. The coefficients $a^{\kappa}_{k_1 k_2}$ are functions of both the angular momenta and the parity of the levels involved. Methods for calculating them in special detection geometries are given by Li 61.

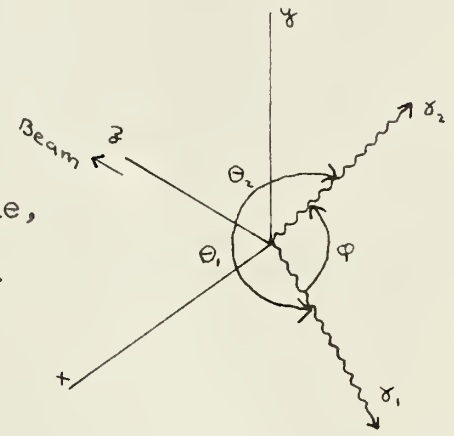


Figure 1-2

In a double correlation, it is often impossible to determine uniquely the angular momenta of the levels involved. (When one is using a bombardment-produced reaction, the double correlation is the distribution of one of the reaction products about the beam direction.) This indeterminacy arises from the possible presence of

several unquantized parameters such as channel spin mixture and orbital spin mixture of the incoming particle and multipole mixing of the outgoing gamma rays. To interpret a double correlation correctly, one must often know these beforehand. However, in a triple correlation, there are so many measurable parameters that these unquantized quantities can be determined by the same experiment.

A Hoogenboom Spectrometer is ideally suited for triple correlation studies.

## SECTION 2. GENERAL DESCRIPTION OF APPARATUS

All the known methods of observing the properties of individual radiations are based on the detection of charged particles. Gamma rays are neutral and therefore can only be detected indirectly by means of interactions in which charged particles are produced. In the energy region of interest here (0-15 Mev.), gamma-ray energy is converted into electron energy through three processes which take place whenever gamma rays pass through matter. The cross-section data given below are for a typical absorber with $A \sim 100$.

1. Photoelectric Effect - cross-section very large at small energies, but rapidly approaching zero around 1 Mev.

2. Compton Effect - cross-section roughly constant at low energies, slowly approaching zero in the region 10 to 100 Mev.

3. Pair Production - cross-section zero below 1.02 Mev. but rising rapidly with increasing energy above this value.

By means of these three processes it is possible to completely absorb gamma rays in matter, converting all

their energy into electron energy. If it were now possible to measure the energy of all the electrons produced, one would indirectly obtain the gamma-ray energy. The most efficient method so far devised for doing this is to use a scintillator as an absorbing medium. Such a material has the property that it is transparent to a certain band of the electromagnetic radiation produced by the electrons coming to rest within it. A NaI crystal, when activated with thallium, has this property. It is transparent to self-produced radiation in the blue region of the visible spectrum. Thus the number of photons of light transmitted by the crystal is approximately proportional to the energy of the electrons stopped and therefore to the energy of the incident gamma ray.

The pulse of light produced is very weak and must be amplified in some way. To this end, a photomultiplier tube is used. This consists of a photocathode and a series of grid elements, called dynodes, arranged at successively higher potentials above the photocathode potential. The photocathode, when struck by photons from the scintillator, releases electrons. These electrons are then attracted to the first dynode and, upon striking it, release more electrons through secondary emission.

Thus electrons produced at the photocathode are attracted to the first dynode, multiplied, attracted to the second dynode, multiplied again, and so on, until finally a very large pulse of electrons hits the anode. (In the photomultiplier used here, the RCA 7046, the current gain is $3 \times 10^6$). The end effect is that each gamma ray which interacts in the scintillator produces a large negative pulse at the anode of the photomultiplier, the amplitude of this pulse being proportional to the gamma-ray energy.

If the output of the photomultiplier is now connected to a multi-channel pulse height analyzer ("kicksorter"), we have a simple gamma-ray spectrometer. The function of the kicksorter is to sort the pulses from the photomultiplier into different groups according to amplitude. The number of pulses in each group is recorded in a corresponding channel of the kicksorter, pulses of smallest amplitude being recorded in the channel of lowest number. The resulting graph of number of counts vs. channel number can be directly interpreted as number of gamma rays vs. gamma-ray energy (see Figure 2-1).

However, this spectrometer is far from ideal. A large number of counts are recorded which correspond to energies less than the actual gamma-ray energy. Furthermore,

the full energy peak ("photopeak") will be much broader than its intrinsic width as defined by the uncertainty principle. The main reasons for these undesirable effects are as follows:

Not all the energy of an incident gamma ray may be collected, for two reasons:

1. A Compton scattered photon may escape from the crystal so that only a fraction of the gamma-ray energy is observed. This gives rise to a "Compton smear" of relatively constant height terminating in a "Compton shoulder" a short distance (0.25 Mev. for a high energy gamma ray) below the photopeak (see Figure 2-1). This shoulder corresponds to the maximum energy an electron can obtain in a Compton scattering event.

2. One or both of the 0.51 Mev. gamma rays resulting from the annihilation of a positron produced in pair production may escape from the crystal. This effect is not important for the low energy gamma rays of Figure 2-1 for which the pair production cross-section is still very small compared to the Compton cross-section but is appreciable at higher gamma-ray energies (see Figure 4-2).

Counts which do not correspond to the whole gamma-ray energy are called "background" counts in the following sections. This is, of course, a misnomer since such counts

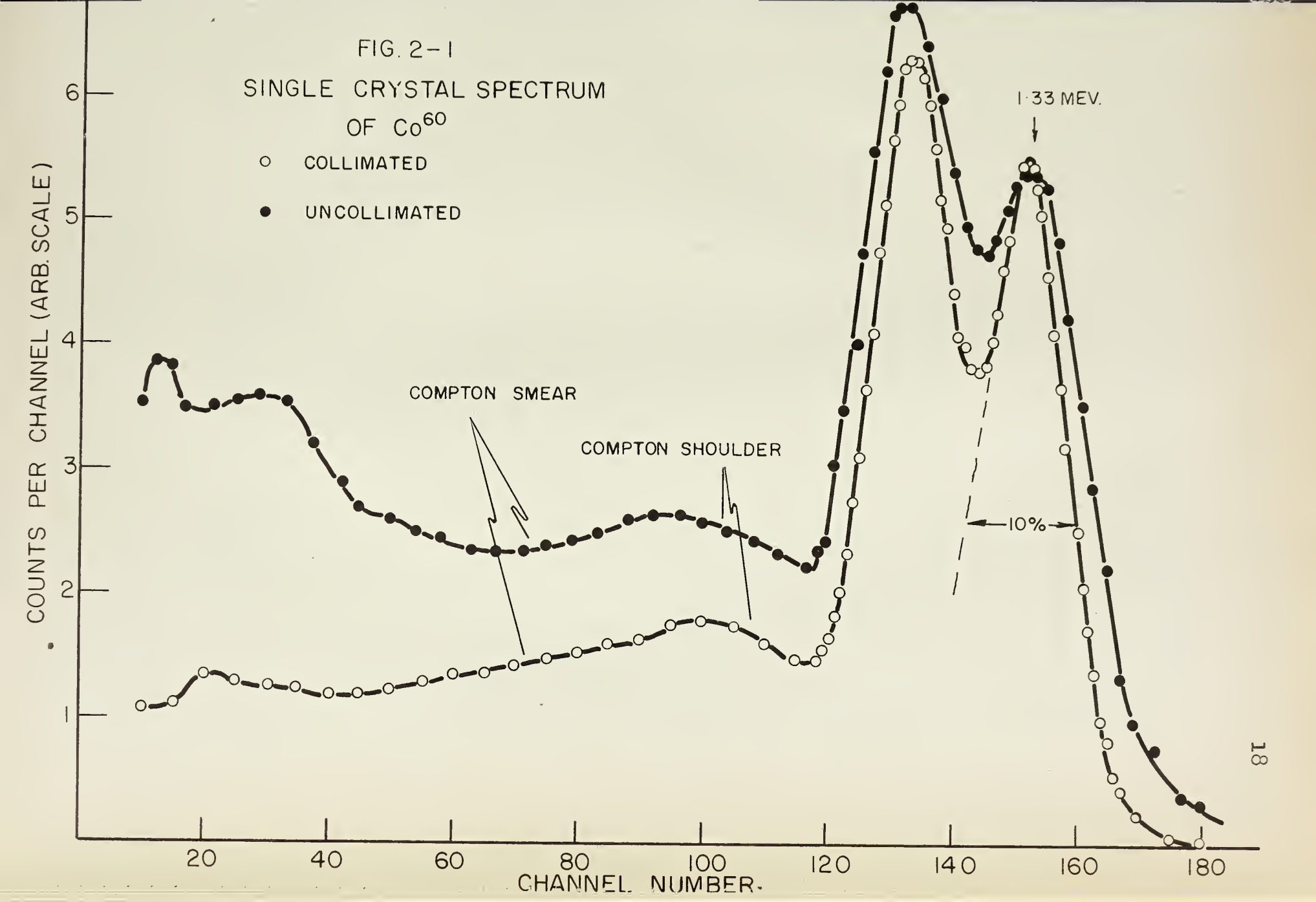
FIG. 2-1
SINGLE CRYSTAL SPECTRUM
OF $Co^{60}$
COLLIMATED
UNCOLLIMATED
1·33 MEV.
COMPTON SMEAR
COMPTON SHOULDER
10%
COUNTS PER CHANNEL (ARB. SCALE)
CHANNEL NUMBER.
1
2
3
4
5
6
20
40
60
80
100
120
140
160
180

can be produced by the gamma ray under investigation.

The second major defect, the broadening of the photopeak and resulting decrease in resolution, is due mainly to the following effects: A variable fraction of the light produced within the crystal is absorbed before it reaches the photocathode. The further an event occurs from the photocathode, the greater the light loss. This effect is magnified by internal reflections and by local concentrations of impurities in the crystal which may increase the absorption in that area. There is also a large loss of resolution in the photomultiplier due to irregularities in the electron-producing properties of the photocathode, and collection and secondary emission properties of the first dynode. Even if both crystal and photomultiplier were perfect, the resolution would be limited by statistical fluctuations in the (small) number of electrons produced at the photocathode.

The smaller the crystal the better the resolution but, on the other hand, the worse the efficiency since a gamma ray can much more readily escape. In choosing the crystal size a compromise must be made between resolution and efficiency.

The background can be greatly reduced by preventing events from occuring near the side of the crystal since

here there is a much higher probability of escape. This is accomplished by collimating the incoming gamma rays. The improvement this produces is shown in Figure 2-1 and the collimation system in Figure 2-2.

Despite the improvement, it is seen that a weak gamma ray may be completely swamped by the Compton smear of a higher energy, more intense gamma ray. Further improvements must be made before one has a gamma-ray spectrometer suitable for high resolution measurements. There are many ways of making such improvements (see for example Kr 60) but only the method used here will be discussed, that due to Hoogenboom (Ho 58).

In its most useful form, this method requires that the reaction under investigation have gamma rays in cascade. Using it, one is able to eliminate almost all the background. However, this is achieved at the cost of a great reduction in efficiency.

To build a Hoogenboom spectrometer, the following additions must be made to the simple spectrometer described above: A second collimater-crystal-photomultiplier combination, an "adding circuit," a differential discriminator, and a gate circuit (see Figure 2-3). The anode outputs of both photomultipliers are fed to the adding circuit, whose output amplitude is proportional to the

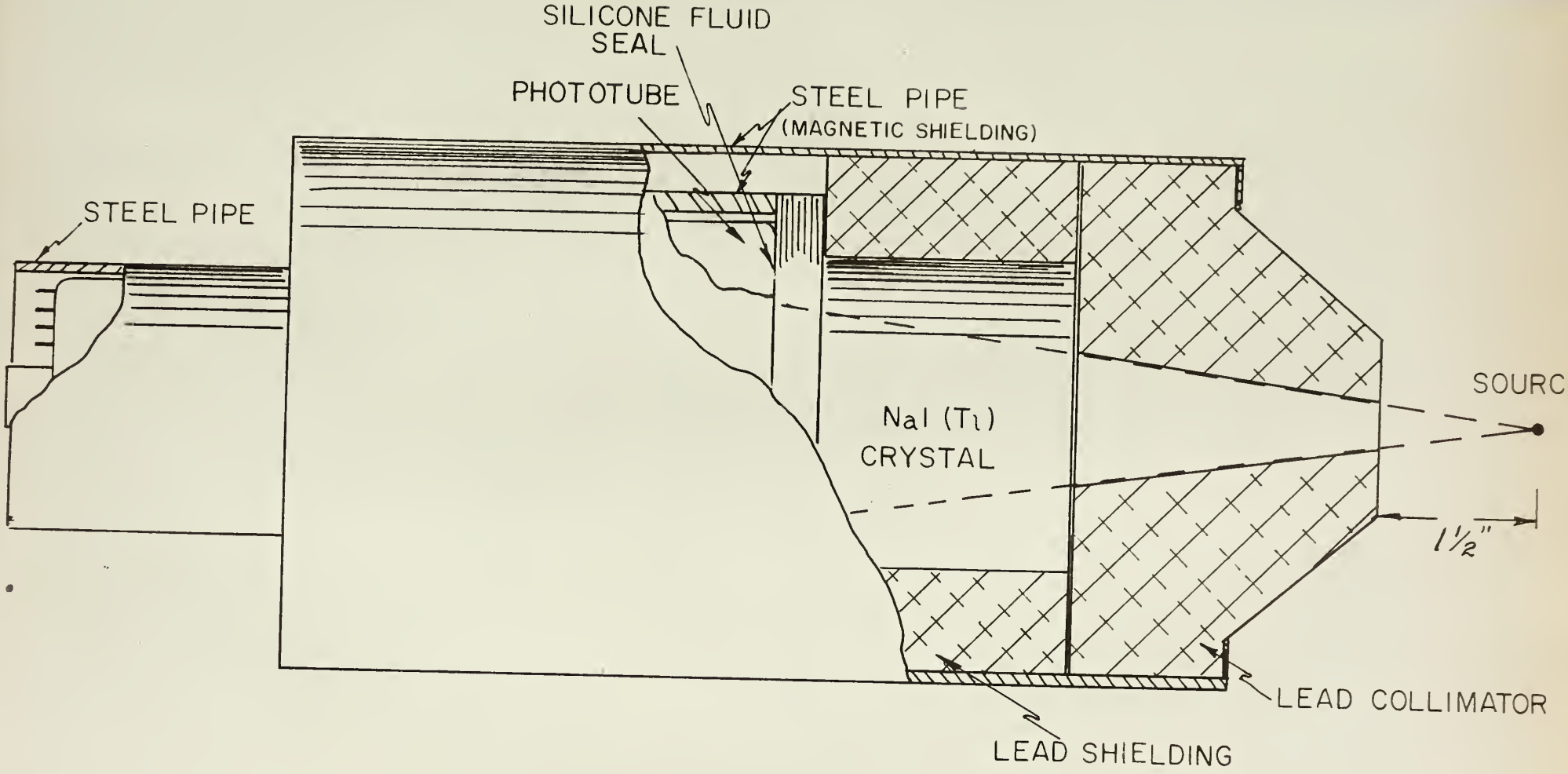


FIG. 2-2 CRYSTAL, PHOTOMULTIPLIER AND COLLIMATION SYSTEM

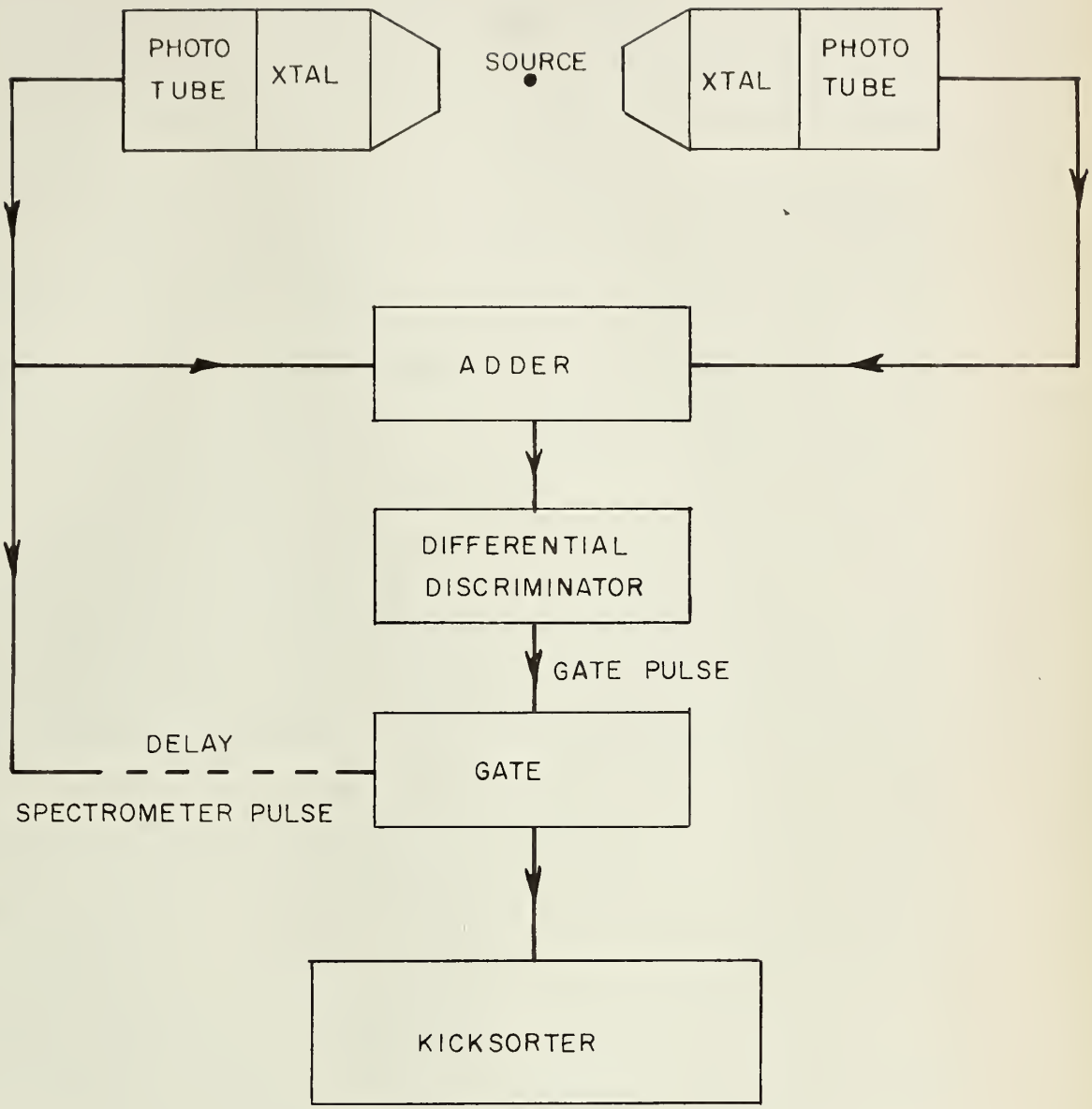


FIG. 2-3
HOOGENBOOM SPECTROMETER
(BASIC CIRCUIT)

total input amplitude (i.e. it adds pulses which are in coincidence). The resulting "sum pulse" is then fed to the differential discriminator which produces an output pulse only if the amplitude of the sum pulse lies within preset limits (i.e. within the "window" of the discriminator). The discriminator output pulse is then used to activate the input circuitry of the kicksorter (i.e. "open the gate" on the kicksorter) allowing one member of the pair of pulses whose sum triggered the gating circuitry to reach the kicksorter.

Suppose we are interested in the gamma-ray decay scheme pictured at right. The differential discriminator is then set to correspond to the total energy $\overline{OB}$, so that whenever gamma rays whose energies add up to this total energy enter the two crystals simultaneously,

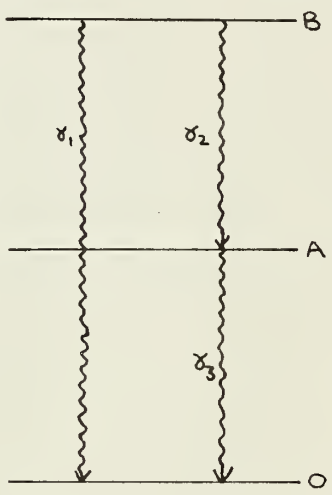


Figure 2-4

the pulse(s) produced in the left-hand crystal of Figure 2-3 are gated on to the kicksorter. A gate pulse is formed whenever $\gamma_1$ is captured in either crystal or whenever $\gamma_2$ and $\gamma_3$ are captured simultaneously in any way by the two crystals. The chance of Compton gamma

rays adding up to the energy $\Theta_B$ is quite small so that almost all the Compton smear will be eliminated. However, because the adding circuit is not a very good coincidence circuit (i.e. it has a long resolving time), there is still an appreciable chance of random pulses adding up to the correct sum. To combat this difficulty, a fast coincidence circuit, operated by pulses from the last dynode of each photomultiplier, is used (see Figure 2-5). Ideally, this circuit produces an output pulse only when two gamma rays from the same event are each captured in a different crystal. Pulses from the fast coincidence circuit and from the sum channel discriminator are fed into a second coincidence circuit which also only produces an output pulse when two input pulses are in coincidence. This output pulse is now used to operate the gate on the kicksorter. Referring again to the schematic cascade of Figure 2-4, it is seen that only when $\gamma_2$ is caught in one crystal and $\gamma_3$, from the same cascade event, is caught in the other will a count be gated on to the kicksorter. $\gamma_1$ will no longer be seen. We see that in general for a count to be registered, the following two conditions must be met:

1. Two gamma rays must be in coincidence.

2. The sum of their energies must lie within the window of the sum channel discriminator.

The Hoogenboom and normal spectra of a $Co^{60}$ source are shown in Figure 2-6.

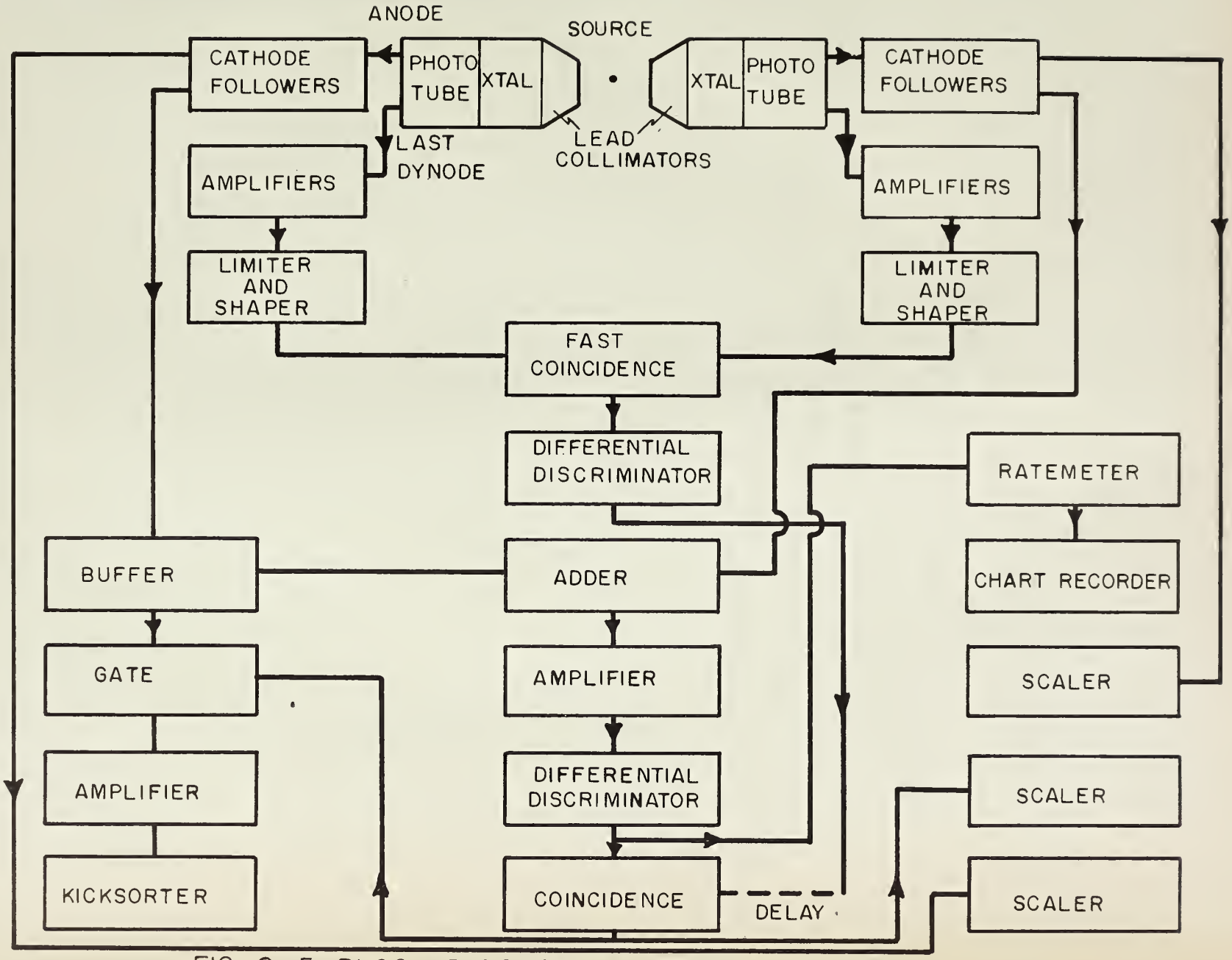


FIG. 2–5 BLOCK DIAGRAM OF APPARATUS

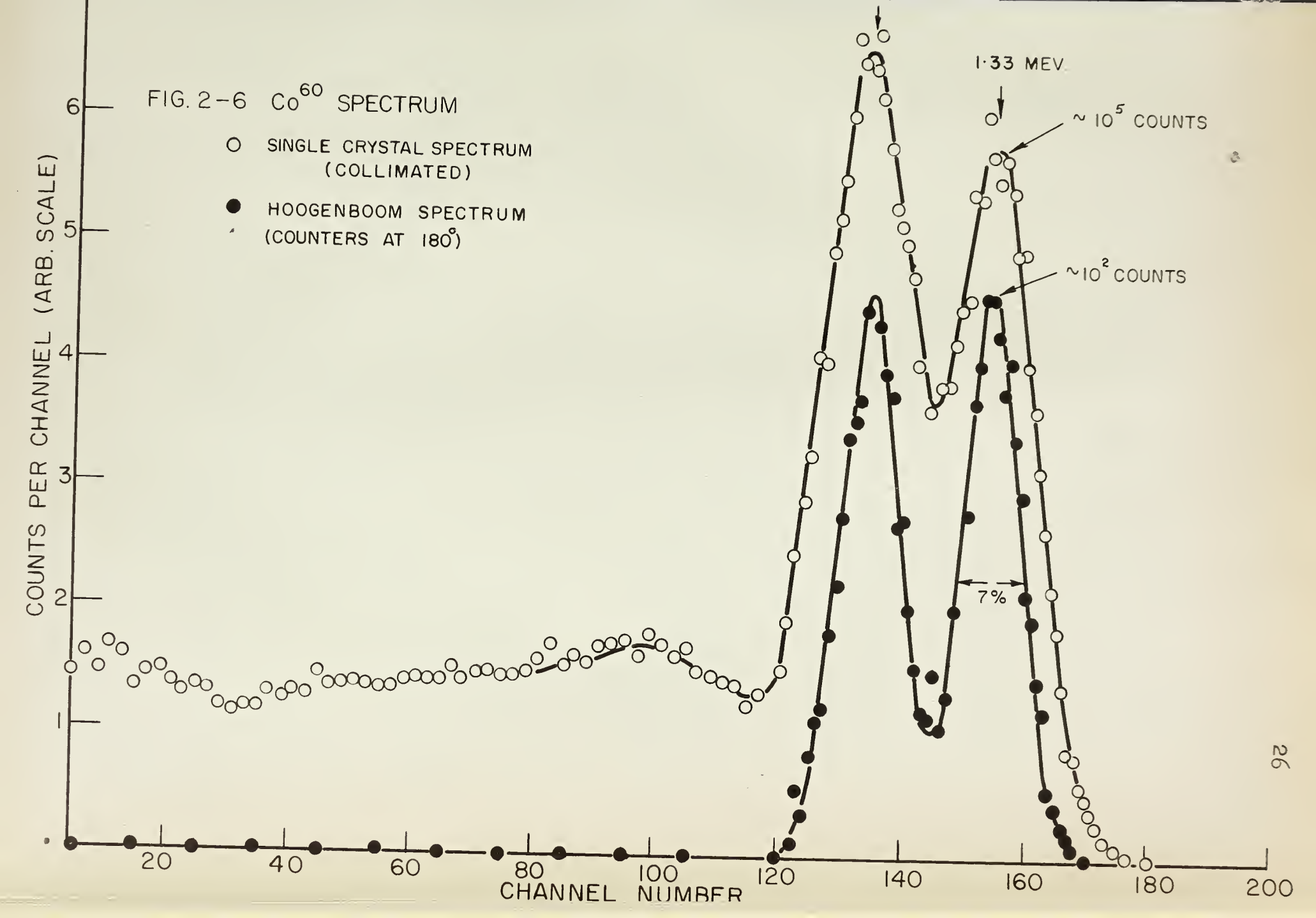
FIG. 2-6 Co60 SPECTRUM
SINGLE CRYSTAL SPECTRUM (COLLIMATED)
HOOGENBOOM SPECTRUM (COUNTERS AT 180°)
1·33 MEV
~ 10^5 COUNTS
~10^2 COUNTS
7%
COUNTS PER CHANNEL (ARB. SCALE)
CHANNEL NUMBER
1
2
3
4
5
6
20
40
60
80
100
120
140
160
180
200

## SECTION 3. EFFICIENCY AND RESOLUTION

### 3-1. Single Crystal Efficiency

The Hoogenboom Spectrometer provides great simplification in the analysis of complex gamma-ray decay schemes but this simplification is achieved at the expense of a very large loss in efficiency. Before discussing this loss, it is necessary to consider the efficiency of a single crystal spectrometer.

Two efficiencies are of importance.

A. Detection efficiency ($\varepsilon_t$): ratio of number of gamma rays of energy E detected (but not necessarily completely absorbed) to the total number of gamma rays of energy E incident on the crystal.

B. Photopeak efficiency ($\varepsilon_p$): ratio of number of gamma rays in the full energy peak of energy $E_p$ to the total number of gamma rays of energy $E_p$ incident on the crystal.

Absolute efficiencies may be obtained by multiplying the above efficiencies by the solid angle $\omega$ (measured in spheres) subtended by the crystal at the source. All these efficiencies are functions of gamma-ray energy and of the geometry of the collimation system.

The detection efficiency can be quite easily calculated.

It is given by

$$\mathcal{E}_t = \frac{1}{2\omega} \int_0^{\tan^{-1} r_2/h_0} [1 - \exp(-\mu t_0 \sec\theta)] \sin\theta \, d\theta$$

where $\mu$ is the linear absorption coefficient of NaI and $t_0$ is the thickness of the crystal ( 4") and the other symbols are as defined on Figure 3-1 which shows the collimation geometry in detail. See Kr 60 for a derivation. The only approximation made in developing this formula is that transmission through and scattering by the collimator body have been neglected.

The detection efficiency has been evaluated from the above formula using a computer and values of $\mu$ as a function of energy obtained from Be 55. The results are shown by curve 1 of Figure 3-2.

To check the theoretical curve, two experimental points have been obtained by the following coincidence method. Suppose two gamma rays in cascade possess an isotropic angular correlation and are detected with efficiencies $\mathcal{E}_{t_1}$ and $\mathcal{E}_{t_2}$ by two identical crystals, each subtending a solid angle $\omega$ . The coincidence counting rate is given by

$$N_{\gamma_1\gamma_2} = 2 N_0 \mathcal{E}_{t_1} \mathcal{E}_{t_2} \omega^2$$

and the counting rate in one crystal is given by

$$N_\gamma = N_0 (\mathcal{E}_{t_1} + \mathcal{E}_{t_2}) \omega$$

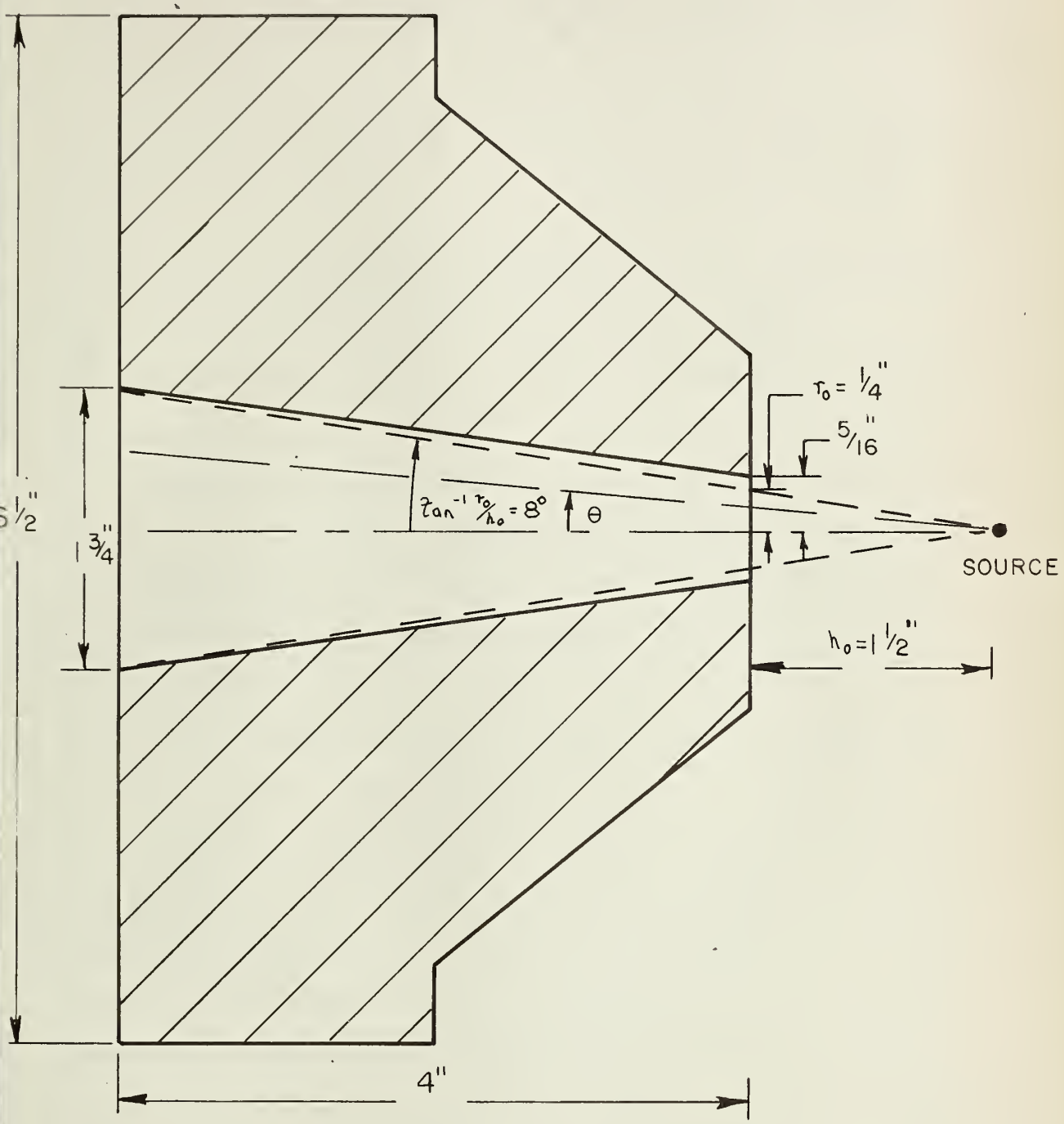


FIG. 3-1 COLLIMATOR DETAIL

where $N_0$ is the number of cascades which take place per unit time interval. Taking the ratio of the two expressions, we have

$$N_{\gamma,\gamma_2}/N_\gamma = 2\varepsilon_{t_1}\varepsilon_{t_2}\omega/(\varepsilon_{t_1}+\varepsilon_{t_2}) .$$

If $\varepsilon_{t_1} \approx \varepsilon_{t_2}$ as is the case for the 1.17 Mev. and 1.33 Mev. cascading gamma rays of $Co^{60}$, this simplifies to give

$$\varepsilon_t \cong N_{\gamma,\gamma_2}/N_\gamma\omega$$

which was the expression used to obtain one experimental point. The $Co^{60}(\beta,\gamma\gamma')Ni^{60}$ shows a strong angular correlation (see Section 5-1) and therefore the above formula is actually invalid. However, the correlation is approximately antisymmetric about 135° (see Figure 5-1) so that at this angle, the effects of angular correlation are nearly cancelled. $Na^{22}$ provided the second point. This source decays by positron emission to the 1.28 Mev. level of $Ne^{22}$. The nearly instantaneous annihilation of the positron results in two 0.51 Mev. gamma rays and one 1.28 Mev. gamma ray per cascade. If the two crystals are located at 180°, exactly facing each other, the situation is somewhat different than above: if one annihilation gamma ray enters the one crystal, the other annihilation gamma ray must necessarily enter the other because of conservation of momentum. However, not all true coincidences recorded will be between annihilation gamma rays. If one annihilation gamma ray is not detected, a coincidence can occur between the other one and the 1.28 Mev. gamma ray from the same event.

Let the number of coincidences produced in these two ways be $N_{\gamma,\gamma_1}$ and $N_{\gamma,\gamma_2}$ respectively, the total being $N_c = N_{\gamma,\gamma_1} + N_{\gamma,\gamma_2}$. Then letting $\mathcal{E}_{t_1}$ and $\mathcal{E}_{t_2}$ be the detection efficiencies of 0.51 Mev. and 1.28 Mev. gamma rays we have

$$\begin{aligned} N_c &= N_{\gamma,\gamma_1} + N_{\gamma,\gamma_2} \\ &= N_0 \mathcal{E}_{t_1}^2 \omega + 2N_0 \mathcal{E}_{t_1} \mathcal{E}_{t_2} (1 - \mathcal{E}_{t_1}) \omega^2 \\ &\cong N_0 \mathcal{E}_{t_1}^2 \omega \end{aligned}$$

and $$N_\gamma = N_0 (\mathcal{E}_{t_1} + \mathcal{E}_{t_2}) \omega .$$

Taking the ratio and solving for $\mathcal{E}_{t_1}$ gives

$$\mathcal{E}_{t_1} = \frac{N_c}{2N_\gamma} \left[ 1 + \left( 1 + \frac{4\mathcal{E}_{t_2} N_\gamma}{N_c} \right)^{1/2} \right] .$$

$\mathcal{E}_{t_2}$ is already known approximately from the result of the $Co^{60}$ coincidence measurement so that the second experimental point of Figure 3-2, curve 1 is obtained.

The photopeak efficiency may also be determined theoretically, but only with much greater difficulty. Thus an experimental method has been used exclusively. Curve 2 of Figure 3-2 represents the ratio of the number of counts in the photopeak to the total number of counts for a number of gamma rays of different energies. Curve 3 of Figure 3-2 shows the actual photopeak efficiency, that is curve 2 corrected by curve 1.

It has already been noted that the formula used in finding the detection efficiency is only approximate; the

FIG. 3-2 SINGLE CRYSTAL EFFICIENCY
FOR
COLLIMATION SYSTEM OF FIG. 3-1

CURVE 1 DETECTION EFFICIENCY THEORETICAL
CURVE 1a DETECTION EFFICIENCY CORRECTED
CURVE 2 RELATIVE PHOTOPEAK EFFICIENCY
CURVE 3 PHOTOPEAK EFFICIENCY
(CURVES 1 & 2 COMBINED)

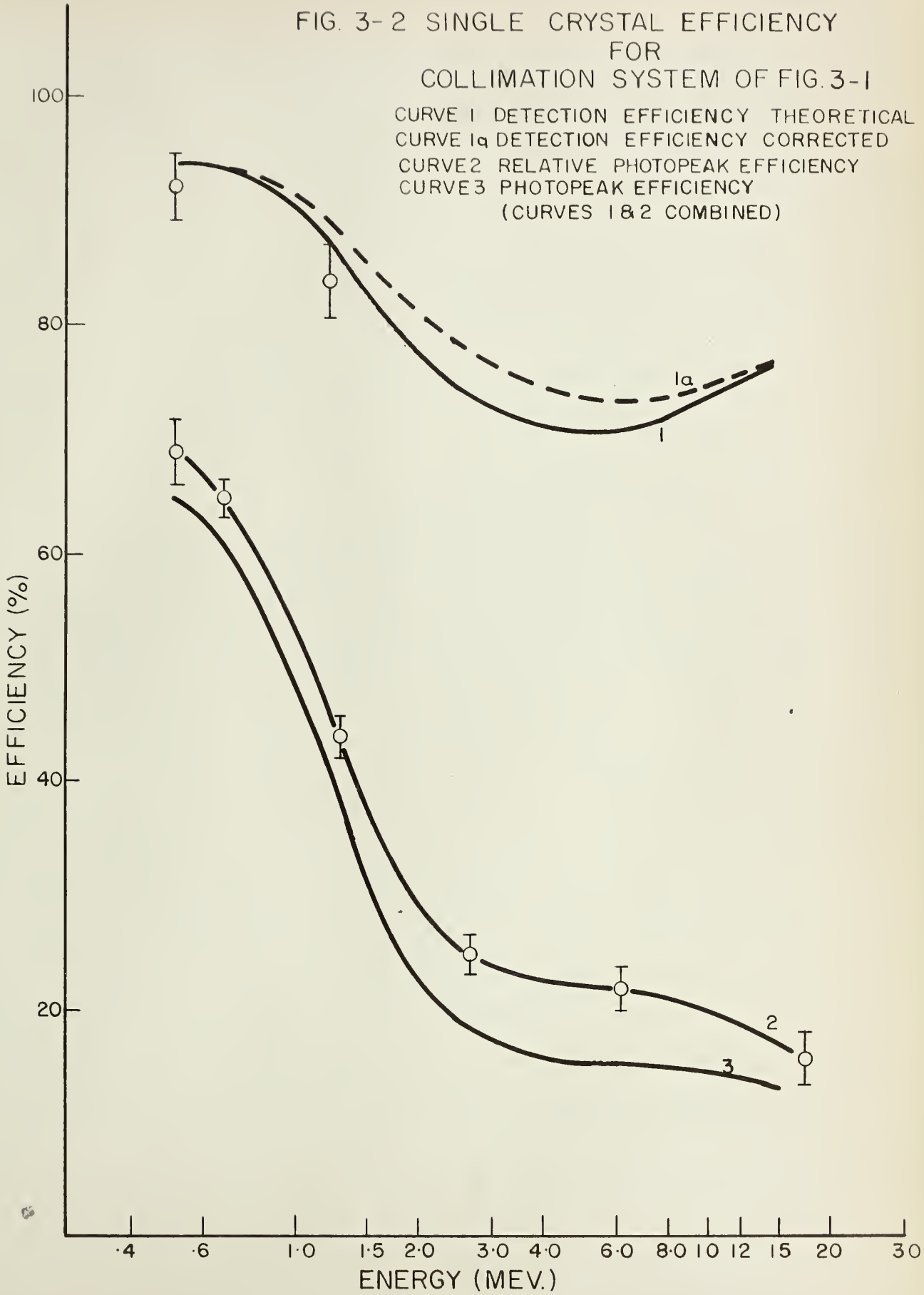

effect of gamma rays penetrating the collimator has been neglected. Let us now see in a semi-quantitative fashion what error this introduces. The minimum in the attenuation coefficient of lead occurs at about 3 Mev. (see Ev 55 for graphs of absorption coefficients). A beam of gamma rays of this energy is 99.2% attenuated and 97.3% absorbed in passing through 4" of lead. However, the collimation system only illuminates about 1/5 of the front surface and 1/3 of the volume of the crystal. Thus a significant number of gamma rays may reach the remaining 2/3 of the volume through the unexposed portion of the front surface of the crystal. To estimate their effect, the unilluminated crystal surface was divided into four concentric zones of equal area and the absorption and attenuation of the gamma rays in the crystal volume behind each area was calculated. At 3 Mev., according to this calculation, the detection efficiency is increased by 4.3%, from about 73% to 77%, and the photopeak efficiency by 1%, from about 18% to 19%. The same calculation was performed for gamma rays of other energies and the corrected detection efficiency so obtained is shown by the dotted line (curve 1A) of Figure 3-2. This calculation actually over-corrects both the detection and photopeak efficiencies since it

was assumed that all gamma rays which pass through the collimator travel in paths radiating from the source. Actually, many of these gamma rays enter the crystal at much greater angles and therefore will escape more easily.

How does "collimator leakage" affect the photopeak efficiency? Curve 3 of Figure 3-2 was obtained by combining curve 1, the detection efficiency for a perfect collimator, and curve 2, the actual ratio of photopeak to background counts. Since curve 2 was obtained experimentally, it contains the effects of the leaky collimator. However, the ratio of total absorption to total attenuation coefficients is about the same in lead and air so any effect produced is small. Thus the photopeak efficiency is a little greater than indicated by curve 3. However, even at an energy of 3 Mev. where the effect is greatest, the correction is a maximum of 1% and therefore was neglected.

Both experimental points of the detection efficiency curve tend to lie too low. This is most likely due to small errors in alignment. Such errors would reduce the coincidence counting rate more than the single crystal counting rate.

## 3-2. Hoogenboom Efficiency

The exact expression for the efficiency of a Hoogenboom spectrometer is quite complicated because of the

rectangular shape of the sum channel window. However, if one approximates this shape by a Gaussian window of the same area, a simple expression is obtained. Suppose $\gamma_1$ and $\gamma_2$ are two gamma rays in cascade with observed energy widths (full width at half maximum) $\Gamma_1$ and $\Gamma_2$ and photopeak efficiencies $\varepsilon_{p_1}$ and $\varepsilon_{p_2}$. Then, as shown by Kr 60, the Hoogenboom efficiency is

$$\varepsilon_H = \varepsilon_{p_1}\varepsilon_{p_2}\Gamma_s\left(\frac{4\ln 2}{\pi}\right)^{1/2} \Big/ \left(\Gamma_1^2 + \Gamma_2^2 + \Gamma_s^2\right)^{1/2}$$

where $\Gamma_s$ is the energy width of the sum channel. The expression is symmetric with respect to the two photopeaks so that they both contain the same number of counts. The absolute efficiency is given by $\varepsilon_H \omega^2$ and is therefore very small. To complete an experiment in a reasonable length of time, a high counting rate is desirable. However, as will be discussed in Section 4, too high a counting rate produces unpredictable gain shifts in the photomultiplier. As a compromise, single crystal counting rates of the order of 10,000 counts per second were usually used.

## 3-3. Resolution

The resolution, R, of a photopeak is defined as the ratio of the width to the energy of the photopeak expressed as a percentage. Single crystal resolution as a function of energy was determined experimentally

and is shown by Figure 3-3. Theoretically, the energy width of a photopeak is given by $\Gamma \cong C E^{1/2}$ where $C$ is a constant. Thus $R \cong C E^{-1/2}$ . Figure 3-3 has been drawn in such a way as to best demonstrate the approximate validity of this relation.

The Hoogenboom resolution is given by

$$\Gamma_{H_1} = \Gamma_1 (\Gamma_2^2 + \Gamma_S^2)^{1/2} \Big/ (\Gamma_1^2 + \Gamma_2^2 + \Gamma_S^2)^{1/2}$$

if one again assumes that the two gamma ray pulse height distributions and the sum channel window may be represented by Gaussian distributions. See Kr 60 for a derivation. The photopeak resolution has been improved over that of a single crystal.

If $\Gamma_S \ll \Gamma_1, \Gamma_2$ then $\Gamma_{H_1} \cong \Gamma_{H_2} \cong \Gamma_1 \Gamma_2 / (\Gamma_1^2 + \Gamma_2^2)^{1/2}$ and the resolution is the same for both photopeaks. Two special cases are of interest.

1. $\Gamma_1 \cong \Gamma_2 = \Gamma >> \Gamma_S$. Then $\Gamma_H = \Gamma/\sqrt{2}$ (See Figure 2-6).

2. $\Gamma_1 >> \Gamma_2 >> \Gamma_S$. Then $\Gamma_{H_1} \cong \Gamma_{H_2} \cong \Gamma_2$. The resolution of the higher energy gamma ray is greatly improved.

In all spectra studied, the agreement between the measured and calculated Hoogenboom resolutions was very close. This provides a justification, albeit a rather weak one, of the special assumptions made about the shapes of the sum channel window and photopeaks.

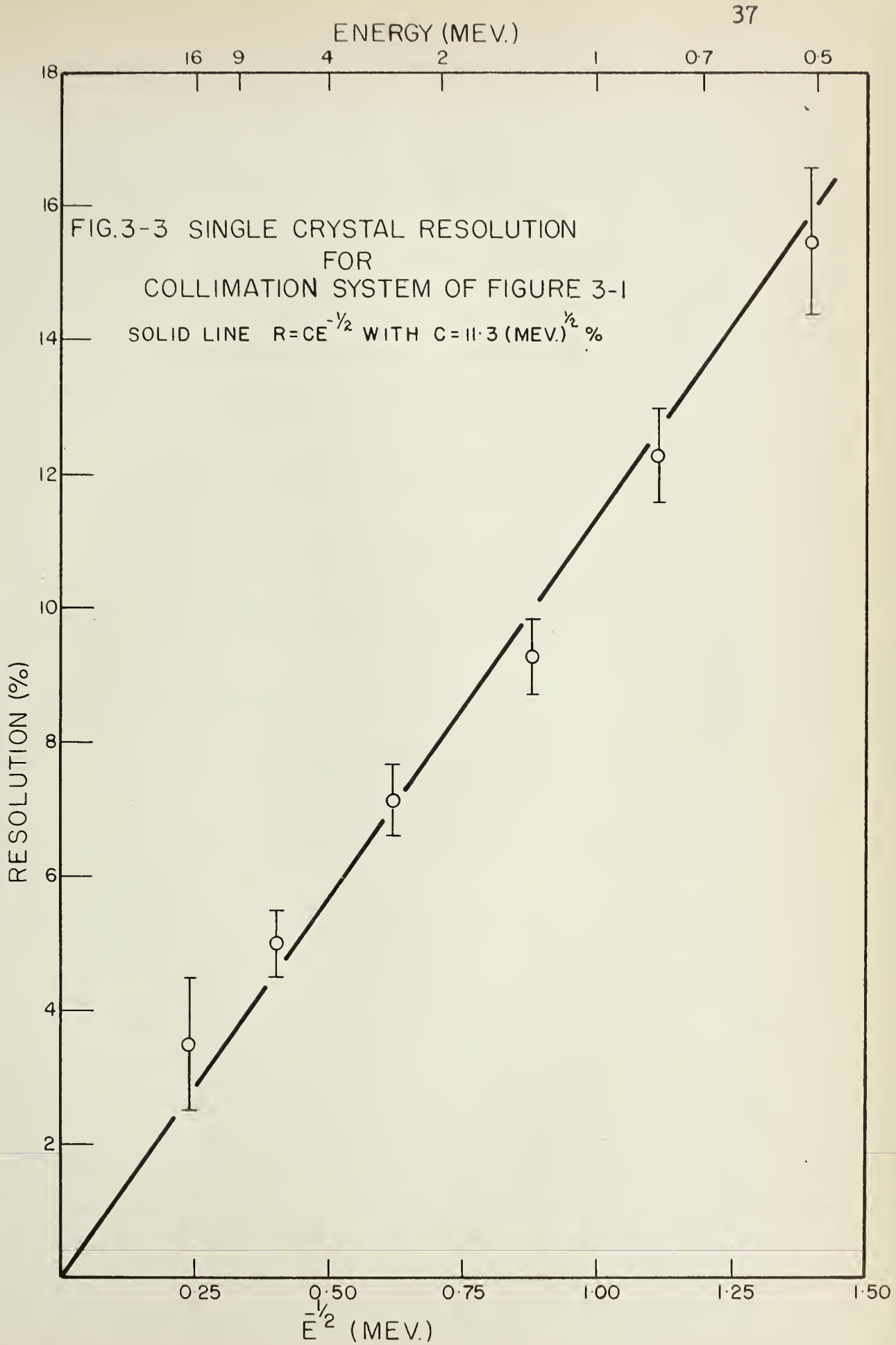


FIG. 3-3 SINGLE CRYSTAL RESOLUTION FOR COLLIMATION SYSTEM OF FIGURE 3-1

SOLID LINE $R = CE^{-1/2}$ WITH $C = 11{\cdot}3\ (\text{MEV.})^{1/2}$ %

3-4. Origins of Random Counts

The fast coincidence circuit eliminates most of the random pulses which, by chance, add up to the correct sum to get through the sum channel discriminator. However, some still manage to do so. Considering a simple $\gamma_1 - \gamma_2$ cascade in which the cascade rate is $N_o$, the number of true coincidences is

$$N_t = 2 N_o \varepsilon_{t_1} \varepsilon_{t_2} \omega^2$$

and the number of chance coincidences is

$$N_c = 2 N_o^2 (\varepsilon_{t_1} + \varepsilon_{t_2}) \omega^2 \tau$$

where $\tau$ is the resolving time of the fast coincidence circuit. The true-to-chance ratio is thus

$$N_t / N_c = \varepsilon_{t_1} \varepsilon_{t_2} / N_o (\varepsilon_{t_1} + \varepsilon_{t_2})^2 \tau .$$

This should be as large as possible, requiring both $N_o$ and $\tau$ to be small. The sum requirement eliminates most of the remainder so that chance coincidences are not a serious problem.

However, if one is looking at gamma rays from low lying nuclear levels, it is quite possible that coincident Compton smear gamma rays from a higher energy cascade will add up to the correct sum. Thus random pulses are gated on to the kicksorter and an appreciable background may result. This background can, of course, be reduced

by narrowing the sum channel window width but not without drastic effects on the counting rate.

Let us estimate the background for the cascade scheme of Figure 3-4. $\gamma_1$, $\gamma_3$ and $\gamma_4$ are each of energy 1.25 Mev. and thus their shapes, if observed separately, would be almost identical to the 1.28 Mev. photopeak of $Na^{22}$; $\gamma_2$ is well represented by the 2.62 Mev. photopeak of Rdth. Figure 3-5 gives the expected shapes of $\gamma_1$ to $\gamma_4$ on the basis of the experimental spectra of $Na^{22}$ and Rdth.

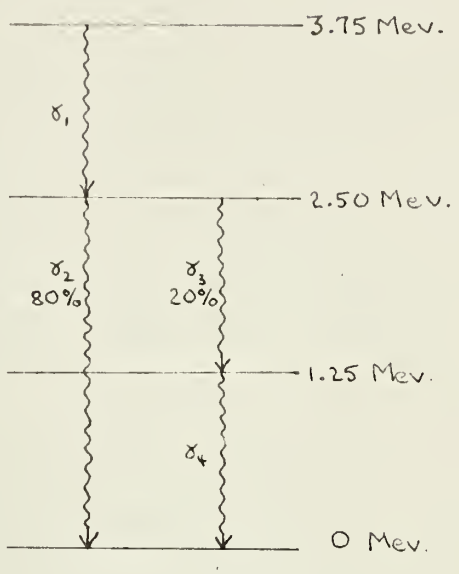


Figure 3-4

Suppose we are interested in the $\gamma_3$-$\gamma_4$ cascade and accordingly set up the gating circuitry to operate on coincident pulses whose sum lies between 2.30 and 2.70 Mev. Coincident Compton events from $\gamma_1$ and $\gamma_2$ may also be of energies adding to this sum. We want to estimate the probability of this happening.

Referring to Figure 7 of Ne 53, which shows Compton cross-section vs. energy of electron produced for a number of different gamma-ray energies, we see that the Compton

cross-section is roughly constant for electrons produced with energies from 0 to $E_\gamma$ -.25 Mev. except for a narrow peak at the high energy end. These high energy electrons, however, correspond to a very low energy scattered gamma ray. This gamma ray is almost certain to be absorbed because of the very large photoelectric cross-section at low energies. The net effect, as seen from Figure 3-5 is that, to a good approximation, the Compton smear may be assumed to have constant amplitude over the entire allowed energy range. Note that this amplitude is approximately the same for $\gamma_1$ and $\gamma_2$ .

The desired probability is found by drawing the graph shown in Figure 3-6. The area enclosing all possible Compton electron energies defines a rectangle. All energy sums within this rectangle occur with equal probability and the probability is one that the sum of Compton events from $\gamma_1$ and $\gamma_2$ should be somewhere within the rectangle. The two slanted lines define the sum channel window width. Thus the probability of the sum lying within the window is the ratio of the finely hatched to the broadly hatched areas, here.132. (In Figure 3-6 the x-and y-axis scales were chosen so that the area enclosing all possible energies is square. This is not actually necessary.)

Figure 3-7 shows the Hoogenboom spectra with background

neglected, and with background shown for sum channel widths of 400 kev. (discussed above) and 40 kev. These curves were drawn using the efficiency and resolution data of Figures 3-2 and 3-3 and the formulae for the efficiency and resolution of a Hoogenboom spectrometer. It should be noted that the background is not directly proportional to the window width because the Hoogenboom efficiency also decreases as the window is narrowed.

The above argument did not give rise to any peaks in the background. However, peaks can and will occur. Suppose, for example, that $\gamma_1$ and $\gamma_2$ are both much greater in energy. Then there is a possibility that the sum of the energies of escape peaks in coincidence might be within the window.

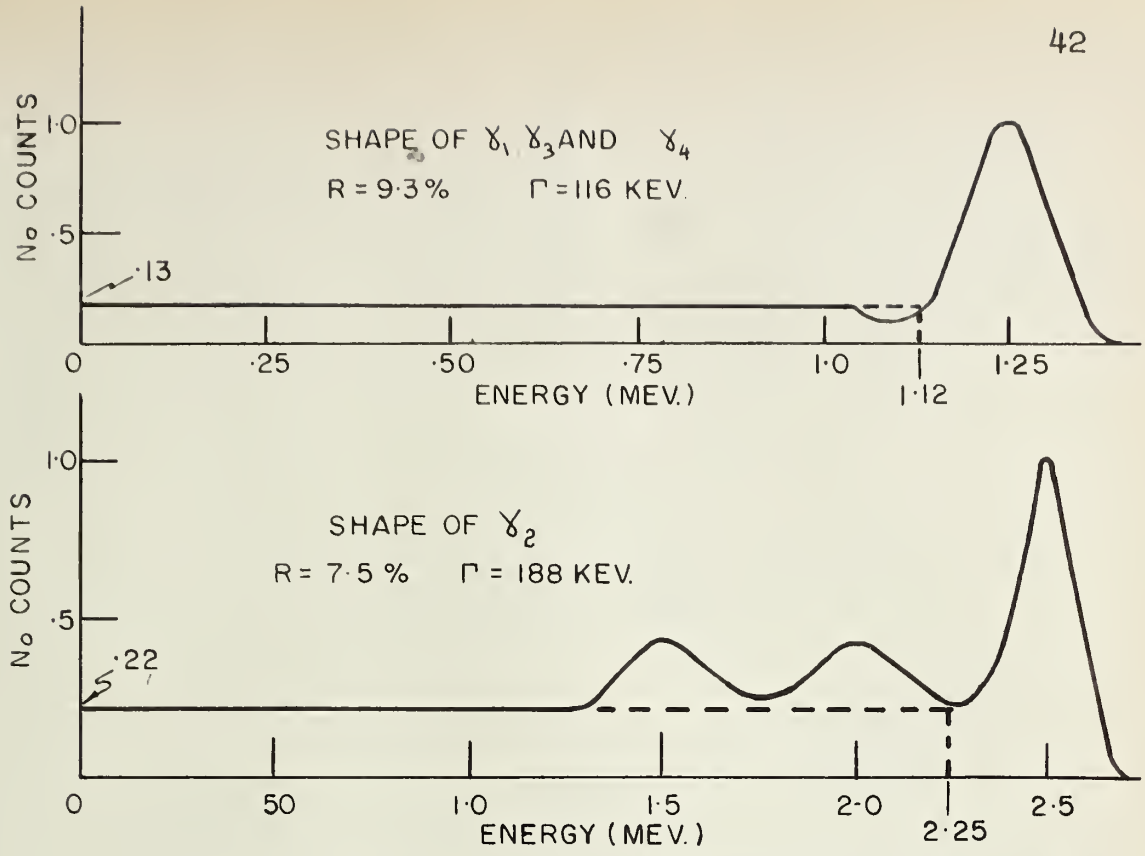


FIG. 3-5 SHAPES OF INDIVIDUAL GAMMA RAYS OF FIG. 3-4

FIG. 3-6 ESTIMATE OF THE PROBABILITY OF THE SUM OF COMPTON ELECTRON ENERGIES FROM $\gamma_1$ AND $\gamma_2$ LYING WITHIN THE SUM CHANNEL WINDOW

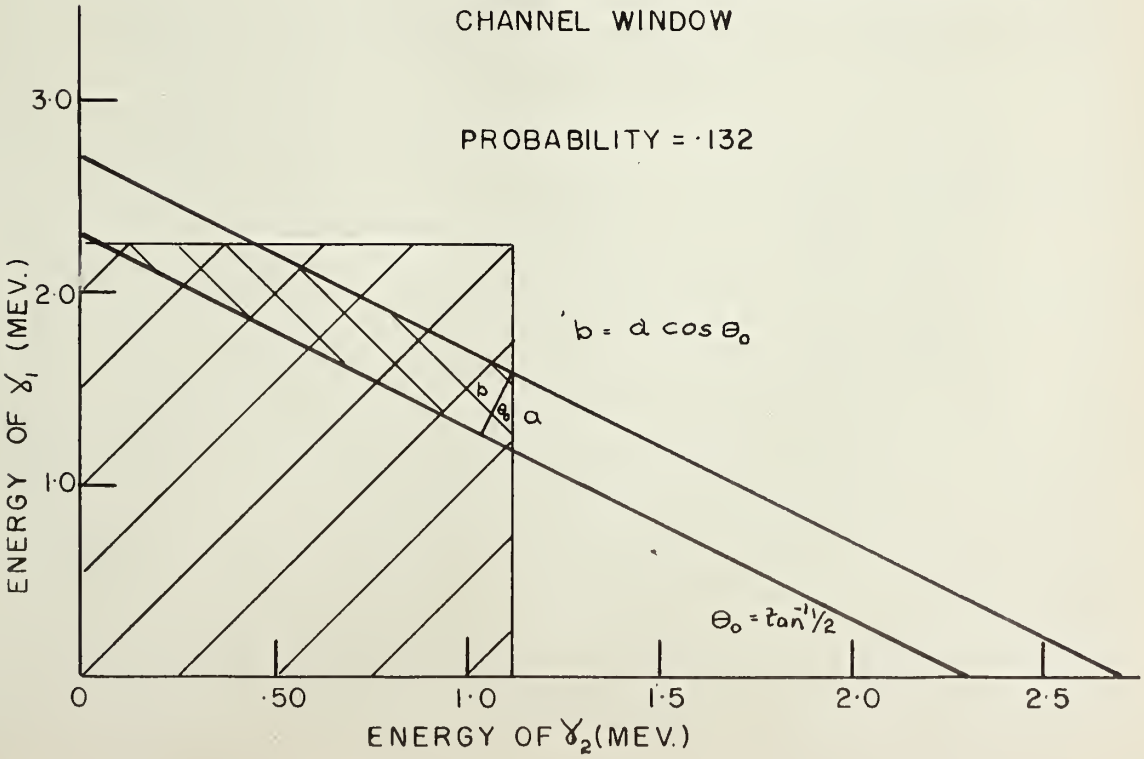

FIG. 3-7 HOOGENBOOM SPECTRUM FOR CASCADE OF FIG. 3-4 WITH SUM ON 2·50 MEV.

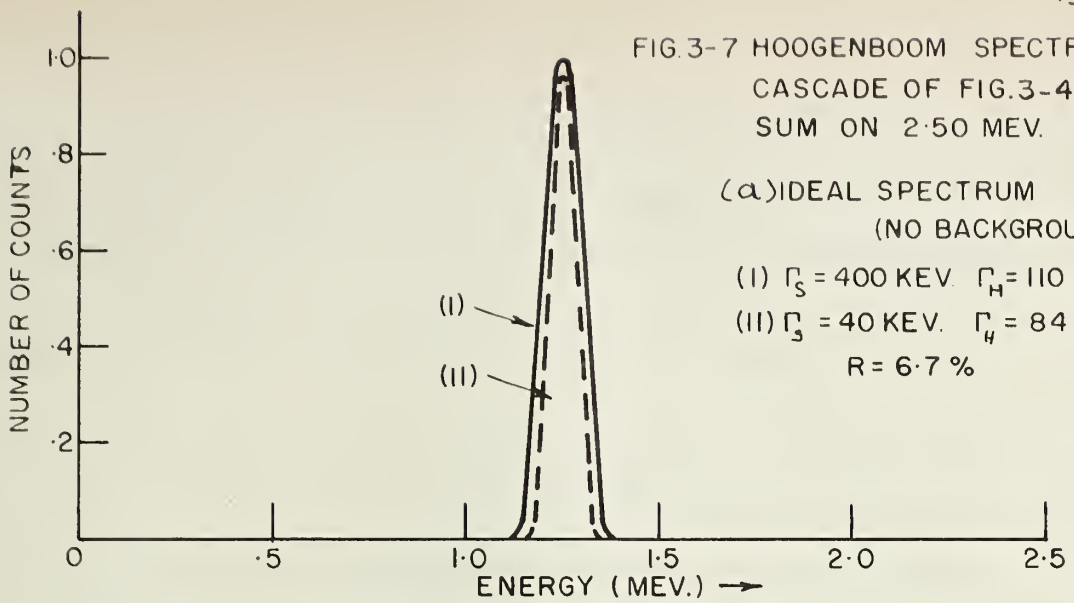


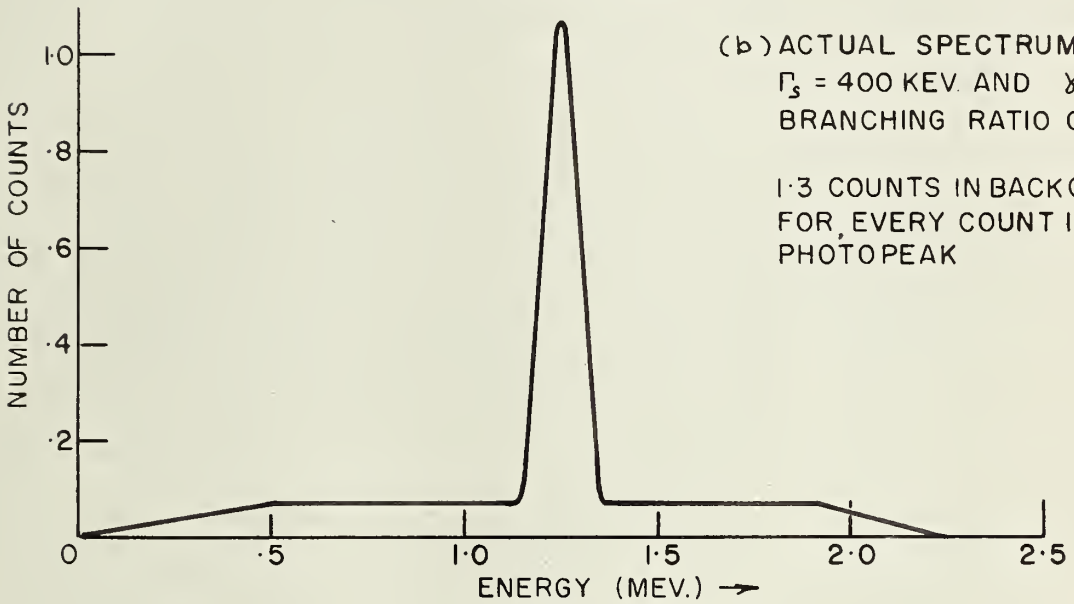


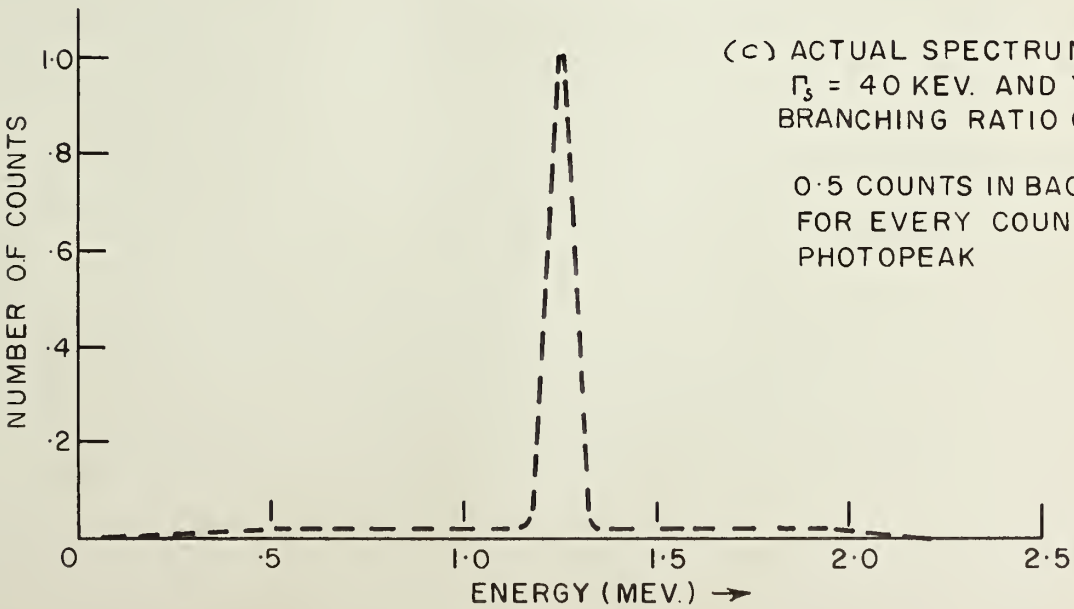

## SECTION 4. SETTING-UP AND ALIGNMENT OF SPECTROMETER

### 4-1. Crystal, Photomultiplier and Header

The heart of the spectrometer is the combination of two thallium-activated 4" NaI crystals each mounted on an RCA 7046 photomultiplier. Two output pulses are taken from each photomultiplier; a negative pulse from the anode to provide the spectrum, operate the adder, and monitor the counting rate; and a positive pulse from the last dynode to operate the fast coincidence circuit. The output impedance of the photomultiplier is matched to the impedance of the output cables by means of three cathode followers in the header, shown in Figure 4-1.

Good optical contact must be made between the crystal and photomultiplier to prevent a serious decrease in resolution. This contact is achieved with Dow-Corning 200 silicone oil which, although extremely viscous, has a tendency to leak out. To slow down this leakage, the photomultiplier is tension mounted on the crystal with a rubber "girdle" made from an old inner tube. To the same end the crystal-photomultiplier combination is kept in a vertical position (i.e. with the contact horizontal) when not in use.

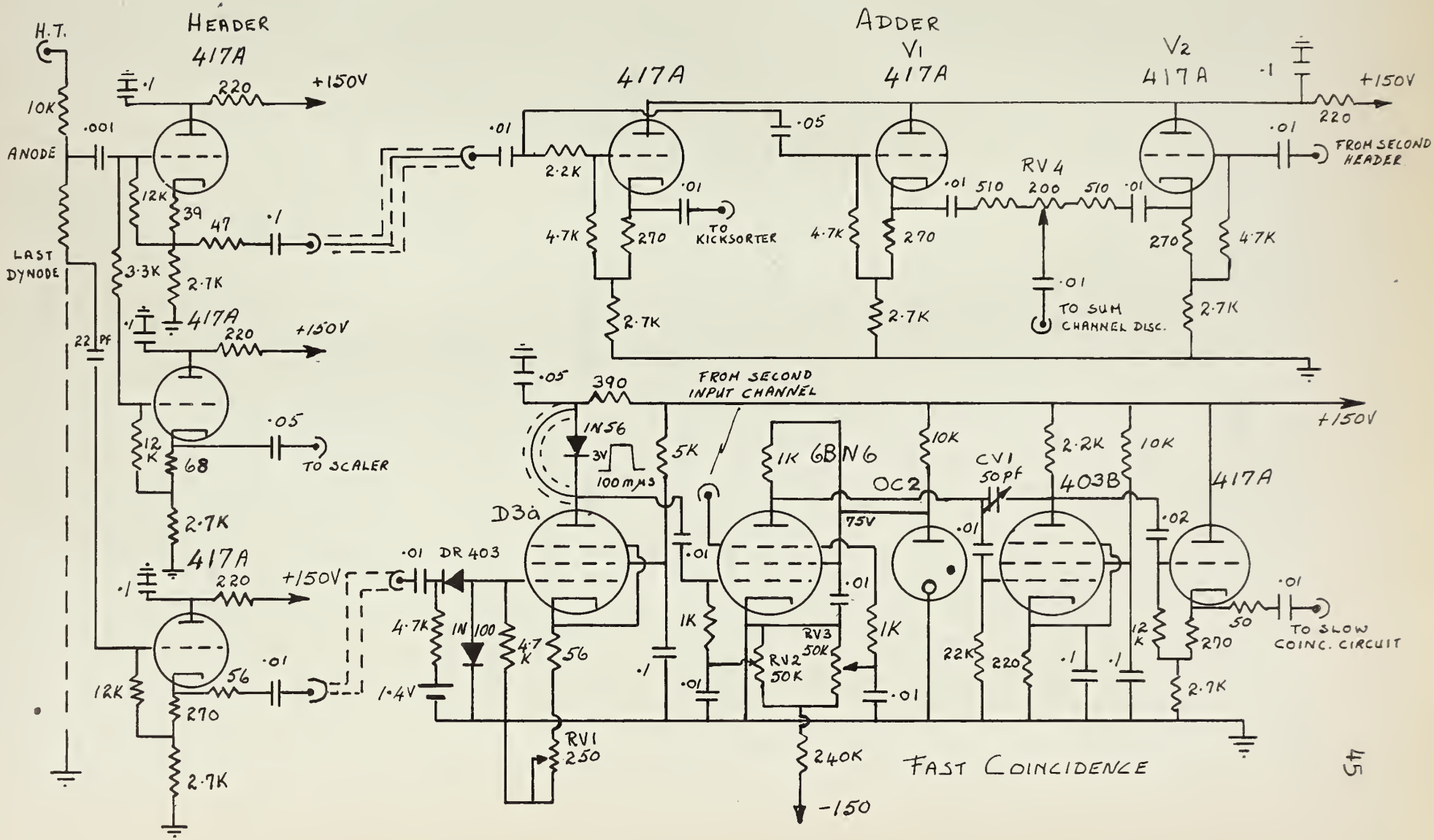


FIG. 4-1 HEADER, ADDER, AND FAST COINCIDENCE CIRCUITS.

(RESISTORS IN OHMS, CAPACITORS IN MICROFARADS, UNLESS OTHERWISE STATED.)

Each photomultiplier casing is periodically checked for light leaks which are sealed with electrical tape and plasticine.

In choosing the best voltage ("H.T.") at which to operate the photomultiplier several things must be kept in mind. First, the dynode pulse must be of large amplitude in order to operate the fast coincidence circuit properly. Secondly, the anode pulse must be of sufficiently small amplitude to maintain linearity both in the photomultiplier and subsequent electronics over the energy range of interest. The photomultiplier output was found to remain linear up to much higher values of the H.T. than the electronics which first becomes non-linear because of overloading of the cathode followers in the sum channel circuitry. Thus, to have linearity in the sum channel while maintaining a large dynode pulse, the anode pulse of the photomultiplier is attenuated. The attenuation is chosen so that the maximum gamma-ray energy of interest corresponds to a 400 mv. pulse at the adder input.

To check the linearity of the electronics, a sliding pulser is used; for the photomultiplier-scintillator combination, gamma rays must be used. Low energy calibration points are provided by standard gamma-ray

sources such as $Na^{22}$(0.51 Mev. and 1.28 Mev. photopeaks) and Rdth (2.62 Mev. photopeak). However, one must go to a bombardment-produced reaction to obtain a higher energy calibration point. The one chosen was $F^{19}(p,\alpha\gamma)O^{16}$ in which higher-energy gamma rays are produced prolifically. A proton bombarding energy of 600 kev. was used because, at this energy, only one gamma-ray transition is strongly resonant, yielding a 6.14 Mev. gamma ray. The single crystal spectrum obtained is shown in Figure 4-2.

There remains one more consideration in choosing the H.T., one which concerns an inherent defect of the photomultipliers. The amplitude of a photopeak of given energy varies with the total counting rate. At a given voltage, this "gain-shift" effect is roughly proportional to both gamma-ray energy and the counting rate. At a smaller voltage the shift is, of course, less. Figure 4-3 shows the effect for the 2.62 Mev. photopeak of Rdth. When the counting rate is suddenly increased, the gain at first rises sharply but then falls exponentially with a time constant of about fifteen minutes to some new lower level. The opposite effect occurs when the counting rate is suddenly decreased, the net result being to produce a sort of "hysteresis loop" as shown in the figure. The existence of this effect means that it is necessary either to maintain a constant counting rate

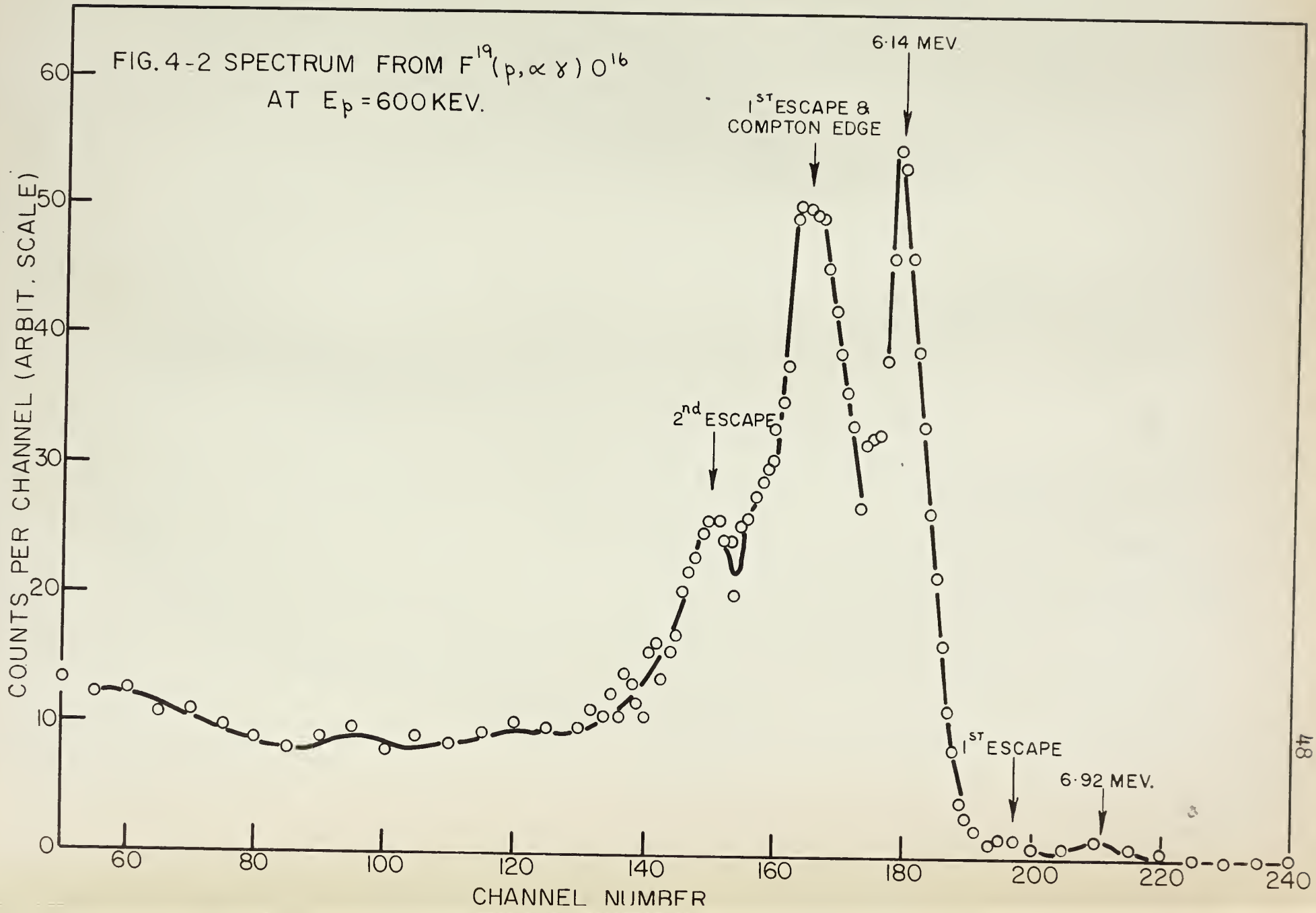
FIG. 4-2 SPECTRUM FROM $F^{19}(p,\alpha\gamma)O^{16}$
AT $E_p$ = 600 KEV.
6·14 MEV.
1ST ESCAPE & COMPTON EDGE
2nd ESCAPE
1ST ESCAPE
6·92 MEV.
COUNTS PER CHANNEL (ARBIT. SCALE)
CHANNEL NUMBER
0
10
20
30
40
50
60
60
80
100
120
140
160
180
200
220
240

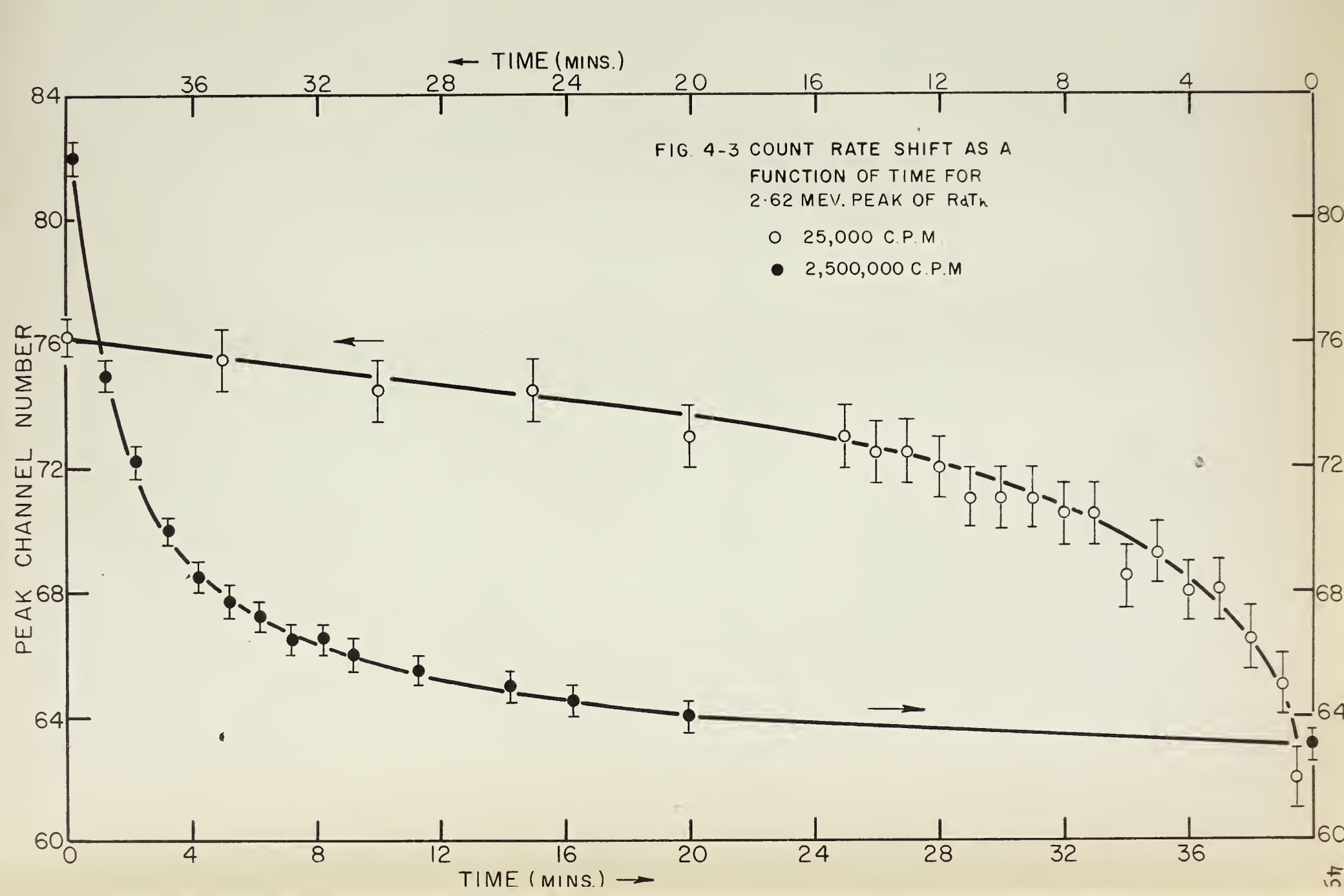
← TIME (MINS.)
36
32
28
24
20
16
12
8
4
0
84
80
76
72
68
64
60
PEAK CHANNEL NUMBER
FIG. 4-3 COUNT RATE SHIFT AS A FUNCTION OF TIME FOR 2·62 MEV. PEAK OF RdTh
O 25,000 C.P.M
● 2,500,000 C.P.M
0
4
8
12
16
20
24
28
32
36
TIME (MINS.) →

throughout any experiment or to use low counting rates ($\sim 5 - 10 \times 10^3$ counts per second) so that gain shifts are not too large. Since the exact magnitude of the gain shift is very hard to predict for a particular situation, a new energy-pulse height calibration is necessary for each experiment. This can be made only after allowing sufficient time for the gain shifts to stabilize. It should be remembered that the gain shift will not usually be the same for two different photomultipliers.

After taking all the above factors into account, the H.T. was set at approximately 1900 volts (but see Section 4-3).

## 4-2. Fast Coincidence Circuit*

Before reaching the fast coincidence circuit (shown in Figure 4-1), the dynode pulses from each photomultiplier are amplified and inverted in two cascaded broad-band amplifiers. The cable lengths used for coupling the broad-band amplifiers to the coincidence circuit are carefully chosen to compensate for differences in internal delay in the two input channels.

A bias battery at the coincidence circuit input is used to clip off noise pulses from the photomultiplier. A diode network eliminates any positive overshoot on

*See Ne 59, from which this circuit is largely copied.

the remaining pulses. The first tube of the circuit is cut-off by the very large ( ~ 100 volts) negative pulses on its grid, thus producing nearly square positive pulses at the anode. These pulses are further squared and greatly shortened by the clipping cable and diode in the plate circuitry of the tube. The result is that all output pulses have a constant amplitude (made to be 3 volts by proper setting of RV1) and a constant length of 100 mμs. set by the clipping cable.

The pulses from the two input channels are now fed to the two grids of the 6BN6. When RV2 and RV3 are set correctly, this tube produces an output pulse only when pulses overlap on its two grids, the length of the output pulse being proportional to their degree of overlap, and the size being related (but not usually proportional) to their amplitudes. Here we see the importance of having large dynode pulses. Only when these pulses are large will they be properly squared so that all input pulses, independent of the energy of the gamma ray which produced them, will be of the same size at the input of the 6BN6. When this is so, the "area" of the output pulse of the 6BN6 is a measure of the true degree of coincidence of the two input pulses.

The 6BN6 output pulse is now integrated by CV1 so that the amplitude of the output pulse of the 403B tube

is proportional to the total charge contained in the input pulse. Thus, the amplitude of this pulse is proportional to the degree of coincidence of the pulses in the input channels. Actually, the proportionality is in general not a linear one but can be made so by careful adjustment of RV2 and RV3. This is achieved by injecting pulses from a pulser into both inputs, delaying one input channel with respect to the other by different amounts and graphing output amplitude vs. delay for different settings of RV2 and RV3 until a linear relationship is obtained as shown in Figure 4-4. Best results were obtained with 6BN6 biases of -3.8v. on $G_1$ and -4.4v. on $G_3$.

The reason for wanting this proportionality is as follows: The resolving time of the coincidence circuit as now described is about 200 mμs. (Twice the length of the input pulses). However, if the pulses are fed to a discriminator whose threshold is set just below the maximum output amplitude, only the very largest pulses will get through. Thus, the resolving time is greatly improved.

Figure 4-5 shows the shape of the coincidence spectra for the 0.51 Mev. annihilation gamma rays from $Na^{22}$ for 0, 20 mμs., and 40 mμs. delay of one coincidence input channel with respect to the other. Clearly, Figure 4-5

FIG. 4-4
RELATIVE AMPLITUDE VS. DELAY, FAST COINCIDENCE CIRCUIT.

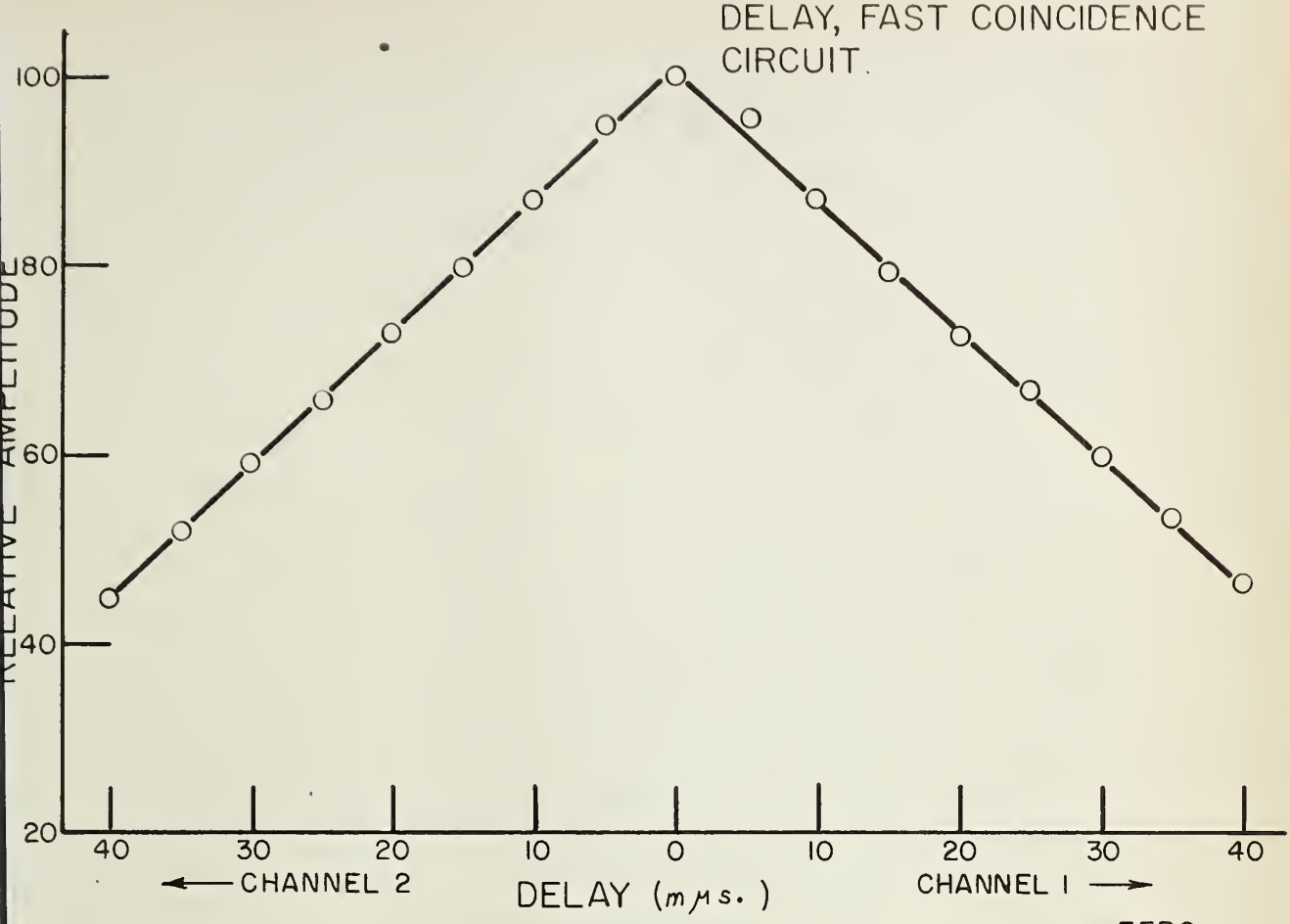


FIG. 4-5
SUPERPOSITION OF COINCIDENCE SPECTRA FOR VARIOUS DELAYS
$\tau \sim 10 m\mu s.$

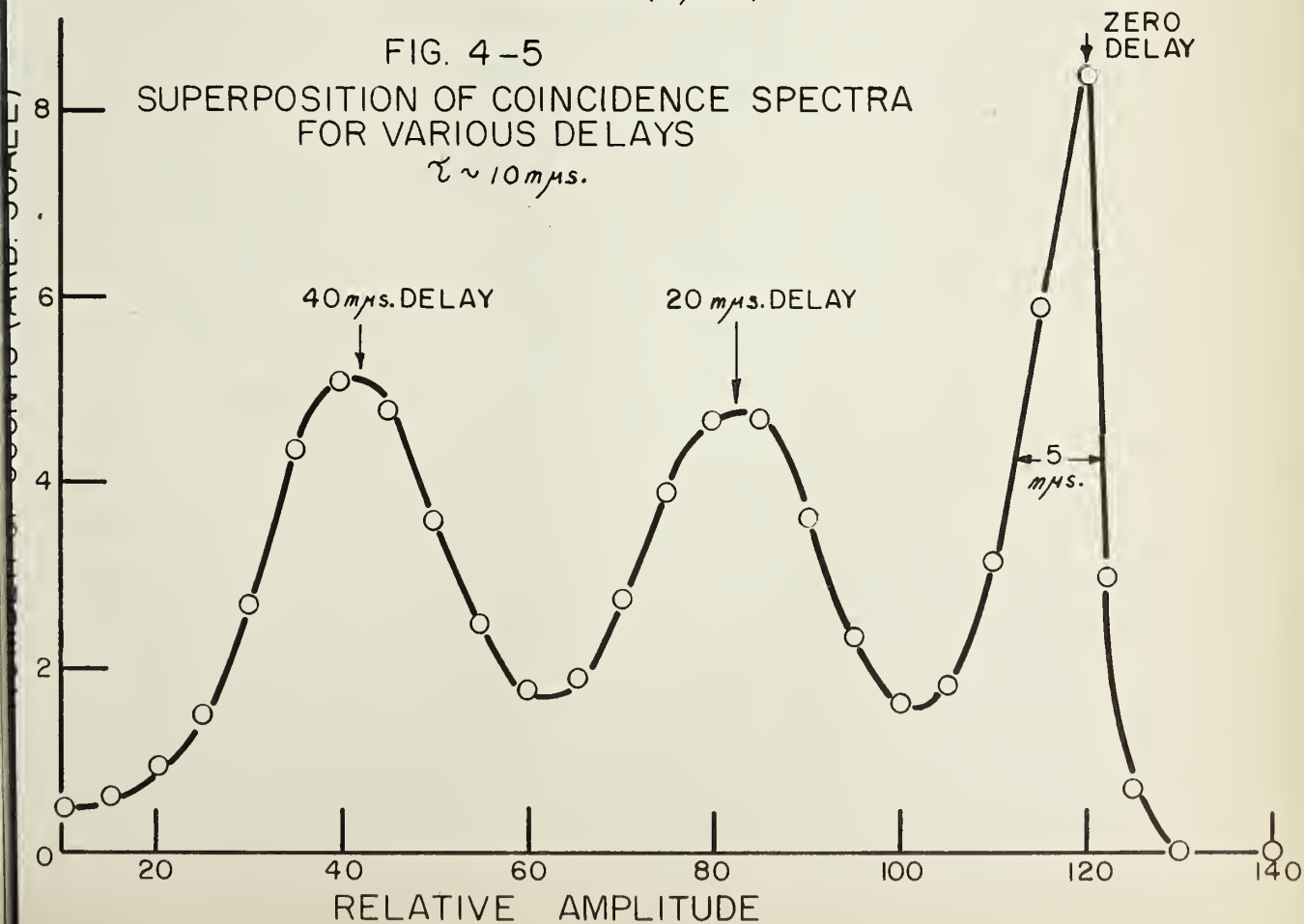

consists of three superimposed spectra. The zero delay peak occurs highest on the kicksorter because it has the largest amplitude. The shape of this peak proves that the delays of the two input channels have indeed been accurately made equal; only if this were so would the zero delay peak have a sharp leading edge. This leading edge corresponds to the greatest output amplitude possible and therefore to pulses in exact coincidence. The few output pulses of even greater amplitude are produced by input pulses piling up on the grids of the 6BN6. The 20 mμs. and 40 mμs. peaks, although produced by pulses of smaller amplitude, are still the result of true coincidences between gamma rays from the same annihilation event. The output amplitude is less because of the artificial delay introduced.

The kicksorter peaks for 20 and 40 mμs. delay contain approximately the same number of counts as the zero delay peak but are twice as broad and, therefore, only half as high. In the zero delay peak, coincident pairs of pulses in which one pulse is either a little bit "late" or a little bit "early" because of time jitter in the photomultiplier and electronics will always result in an output pulse whose amplitude is less than the "exact zero" amplitude. The situation is different for the delay peaks. Here, if that member of a coincident pair of

pulses in the delayed input channel is "early," the output amplitude will be greater than for a pair of pulses unaffected by time jitter. The opposite is true for a late pulse in the delayed input channel.

The position on the kicksorter of the 0, 20 and 40 mμs. delay peaks establishes a time scale, enabling the determination of the resolving time of the circuit: it is twice the half-width (we are delaying only one input) of the zero delay peak, here about 10 mμs.

The resolving time of the spectrometer is checked periodically. When studying deuteron-induced reactions, this can be done very easily by making use of the carbon contamination of the target (which is almost certain to be there, despite all precautions). Because of this contamination, the reaction $C^{12}(d,n)N^{13}(\beta^+)C^{13}$ takes place and two annihilation photons are produced. If the counters are set at $180^{\circ}$ with respect to one another and the sum channel is set at 1.02 Mev., the resolving time can easily be determined by the procedure used to obtain Figure 4-5. One must work fairly quickly since the half life of $N^{13}$ is only ten minutes.

The annihilation gamma rays resulting from the carbon contamination also provide the most convenient way of making sure that the two crystals are seeing the same part of the target. The two counters are again

placed at 180° with respect to one another and one counter is moved up, down and sideways until the coincidence counting rate is a maximum.

4-3. Sum Channel

The adding circuit is shown in Figure 4-1 and is essentially just three cathode followers. For the adder to work properly, the inputs of $V_1$ and $V_2$ must be almost identical in size and shape. This can be accomplished by fine variations in the H.T. and by suitable choice of coupling capacitors. Any remaining differences in amplitude at the adder output can be removed by proper adjustment of RV4. This is most easily done by displaying the adder output on the kicksorter with only one input connected at a time and adjusting RV4 until the spectra are identical. The adder balance is checked in this way before each run.

The sum channel discriminator is calibrated before each run. The threshold potentiometer of this discriminator is connected to a small motor, allowing the window to be swept mechanically over the whole spectrum. For calibration, the discriminator output is connected to a ratemeter which is in turn connected to a chart recorder. The mechanical drive is used to sweep across the whole sum spectrum so that a graph of number of counts vs.

threshold setting is obtained on the chart recorder, enabling one to identify the threshold setting for a desired gamma-ray energy.

The exact width of the window is checked periodically with a sliding pulser.

## 4-4. Slow Coincidence Circuit

Diagrams and the theory of the operation of the slow coincidence circuit may be found in Kr 60. In essence, it is much the same as the fast coincidence circuit already described. Each input channel contains a threshold amplifier which can be used as a discriminator and a flip-flop circuit for producing pulses of constant amplitude and length to be fed into a 6BN6. These pulses are made to be 4 volts in amplitude and any desired length greater than or equal to 100 mμs. The output channel is adjusted to produce gating pulses 9 volts high and 1 to 3 μsec. long to operate the gate on the kicksorter.

The discriminator used to improve the fast coincidence resolving time is contained in the slow coincidence circuit. To facilitate its setting, the pulses from the fast coincidence circuit are amplified. Small variations in fast coincidence resolving time are accomplished with small variations in the fine gain of

the amplifier rather than varying the threshold setting of the discriminator.

The delays in the sum and fast coincidence input channels were made equal with 100 Ω lumped delay line.

The resolving time of the slow coincidence circuit is set at about 100 mμs. This resolving time is also checked periodically.

Section 4-5. List of Equipment Used

Spectrometer

| | | |
|---|---|---|
| Photomultipliers | 2-RCA 7046's | |
| Crystals | 2-NaI(Tl) 4"x4" cylindrical crystals | Harshaw Chemical Co. |
| H. T. Supply | Model 408A | John Fluke Mfg. Co. Inc. |
| Dynode pulse amplifiers | 2-Type AR<br>2-Type BR<br>broad band amplifiers | Hewlett-Packard Co. |
| Fast coincidence adder and header circuits | as described | |
| Sum channel discriminator | SC76 M spectrometer | Tracerlab Inc. |
| Ratemeter | SC79 | Tracerlab Inc. |
| Chart-recorder | Recti/Riter | Texas Instrument Co. |
| Fast coincidence amplifier | Model 204B | Baird-Atomic, Inc. |
| Slow coincidence circuit | Kr60 | |
| Scalers | 1-Model SC 700<br>1-Model SC 750<br>1-lab built scaler | Eldorado Electronics |
| Lumped delays | | Valor Instruments, Inc. |
| Power supplies<br>A.C. regulator | 5<br>1 | Lambda Electronics Corp.<br>General Radio Co. |

Recording Equipment

| | | |
|---|---|---|
| Kicksorter | Model 220 data output unit<br>Model CN110 digital computer unit<br>Model 210 pulse height logic unit | Technical Measurement Corp. |
| Printer | Model 561B digital recorder | Hewlett Packard Co. |
| Plotter | Variplotter | Electronic Associates Inc. |
| Plotter control | Model 326A dual preset controller | Computer Measurements Corp. |

## SECTION 5. RESULTS AND DISCUSSION

### 5-1. Angular Correlation of the $Ni^{60}$ $\gamma$-$\gamma'$ Cascade.

The angular correlation of the gamma-ray cascade in the reaction $Co^{60}(\beta^-, \gamma\gamma')Ni^{60}$ has been measured with the Hoogenboom spectrometer. This particular angular correlation has been measured many times and the agreement between theory and experiment is very good (for example, see K153). Thus the object of this experiment was to demonstrate the feasibility of using the apparatus for angular correlation studies rather than learning anything new about the $Ni^{60}$ cascade.

The experimental procedure was as follows. The number of coincidence counts in the two gamma-ray photopeaks of the Hoogenboom spectrum was measured for a fixed time interval at seven different angles, the spectrum being obtained from the movable crystal. At the same time, the total number of counts occuring in the individual crystals was measured.

The number of coincidence counts was corrected in two ways. First, the number of chance coincidences in

the photopeaks was subtracted from each reading. This was determined by inserting 50 mμs. of delay in one channel of the fast coincidence circuit (a delay sufficient to eliminate all true coincidences) and repeating one run. Secondly, a first-order correction for source non-alignment was made by dividing the number of coincidence counts by the ratio of the total number of counts in the movable crystal to the total number of counts in the fixed crystal.

The corrected coincidence counting rate is plotted in Figure 5-1.

The coefficients $a_{2n}$ of equation ⑨ Section 1 are best found from the experimental data by the method of least squares. The standard method, discussed in great detail by Ro53, involves inverting an $n \times n$ square matrix where $n$ is the number of experimental points. The errors on the coefficients are obtained from the analysis. A subtler method (Ha51) involves inverting an $n' \times n'$ triangular matrix where $n'$ equals the number of terms in series ⑨. This is the method used here. Although much simpler to apply, it has the serious disadvantage that no estimate of the error is obtained.

For convenience, let us expand ⑨ in powers of cos θ rather than Legendre polynomials. Then, taking $n_{max} = 2$,

$$W(\theta) = \text{const.} \left(1 + b_2 \cos^2\theta + b_4 \cos^4\theta\right) .$$

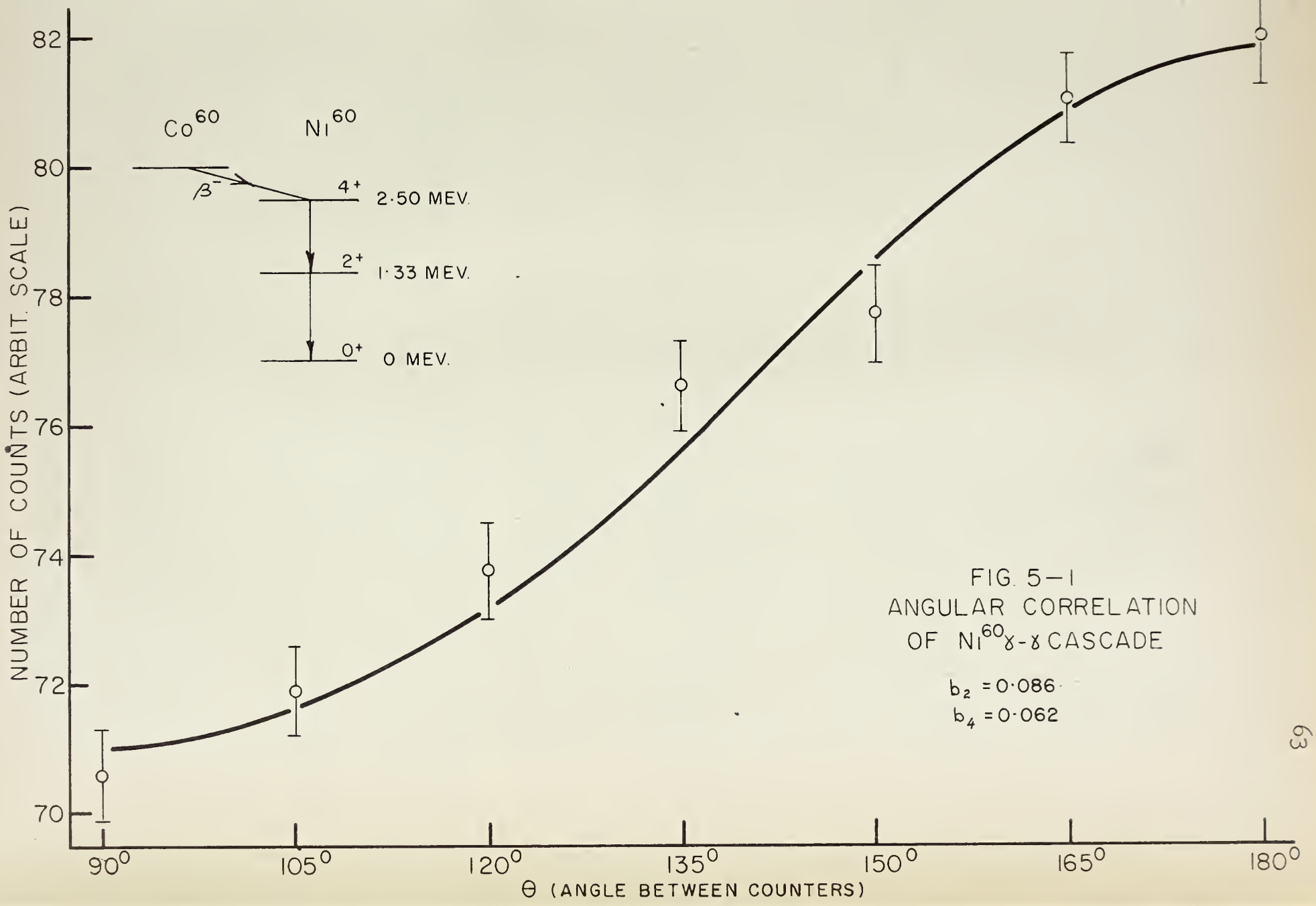


FIG. 5—1
ANGULAR CORRELATION
OF $Ni^{60}$ γ-γ CASCADE

$b_2 = 0{\cdot}086$
$b_4 = 0{\cdot}062$

Analysis of the data gives

$$b_2' = .086 \quad \text{and} \quad b_4' = .062 \ .$$

The primes are used because these coefficients are not quite the same as the theoretical coefficients; the experimental coefficients are influenced by the finite solid angle subtended by the crystals. The theoretical coefficients can be corrected to include this effect. In terms of the $a$'s, the correction is crudely given by (see Wa50).

$$a_2' = (1-6\omega)a_2 \qquad a_4' = (1-20\omega)a_4$$

where $\omega$ is the solid angle, in spheres, subtended by the crystal. The theoretical $b$'s are then found from the $a$'s and are

$$b_2' = .123 \qquad b_4' = .037 \ .$$

The least squares fit here obtained is plotted in Figure 5-1.

The agreement between the theoretical and experimental coefficients does not appear to be too good, probably for two reasons: the point at $150^\circ$ appears too low, a deviation which could be caused by statistical fluctuations. Also there were some serious experimental difficulties which will be described shortly.

The secret of performing a good angular correlation experiment is twofold: one's electronics must be stable,

and one must be able to position the source accurately. Little trouble was had with the first requirement but almost insurmountable difficulties were had with the second. The fault lay with the stand, which had been originally designed for another purpose. Its arms moved in and out according to their angular separation. A flimsy floor, designed to reduce neutron background, did not help either: the whole stand swayed back and forth whenever anyone came near it. The motions of the stand were actually rather small but the crystals were so close to the source and the collimator openings so narrow that the stand's motions were capable of introducing an artificial correlation of 5%.

The only way in which the $Ni^{60}$ cascade correlation could be measured even approximately was by attaching the $Co^{60}$ source firmly to the stand. In this way, the source remained nearly centered despite the motions of the stand. Obviously, the first requirement for future angular correlation studies is a sturdy stand. This should be built so that both the polar and azimuthal angular separation of the detectors can be varied quickly and accurately. Such a stand has been designed and will soon be built.

Triple correlations experiments, although the original intention, were made impossible by the inadequacies of the stand.

5-2. Yield Curve Measurements

The yield of cascading gamma rays from three levels of $B^{10}$ formed in the reaction $Be^{9}(d,n\gamma)B^{10}$ has been measured using the Hoogenboom spectrometer. This was done in an attempt to observe a reported resonance in the reaction rate cross-section around 1 Mev. (see Sh57). Figure 5-2 (taken from Aj59) shows the gamma-ray decay scheme of the lower levels of $B^{10}$ and Figure 5-3 shows the single crystal gamma-ray spectrum of $B^{10}$ + d. Figure 5-4 shows the measured yield curves. All points on these yield curves were obtained using the detection geometry of Figure 5-7.

To interpret Figure 5-4, let us consider the gamma rays from each level of $B^{10}$ in turn (see Figure 5-2).

0.72 Mev. level: Since this is the first excited state, only the gamma-ray transition to the ground state is present. Thus a Hoogenboom spectrum cannot be obtained.

1.74 Mev. level: This level decays entirely by a single cascade through the 0.72 Mev. level and thus the spectrometer, with the sum channel set at 1.74 Mev., measures the total gamma-ray yield.

2.15 Mev. level: This level can decay to the ground state via three different routes, but only one of these produces two gamma rays in cascade with total energy 2.15 Mev.

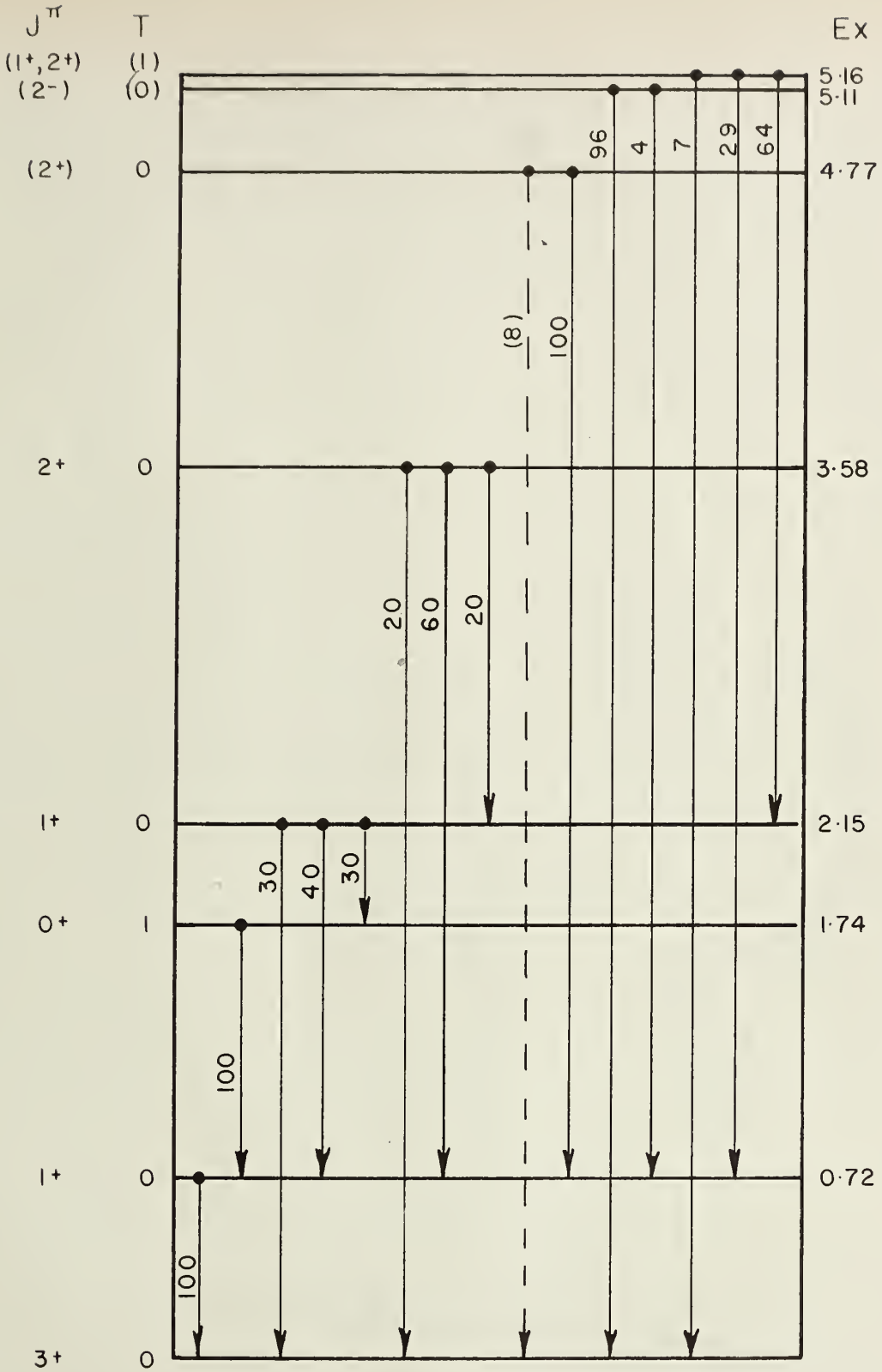


FIG. 5–2 LEVEL DIAGRAM OF $B^{10}$

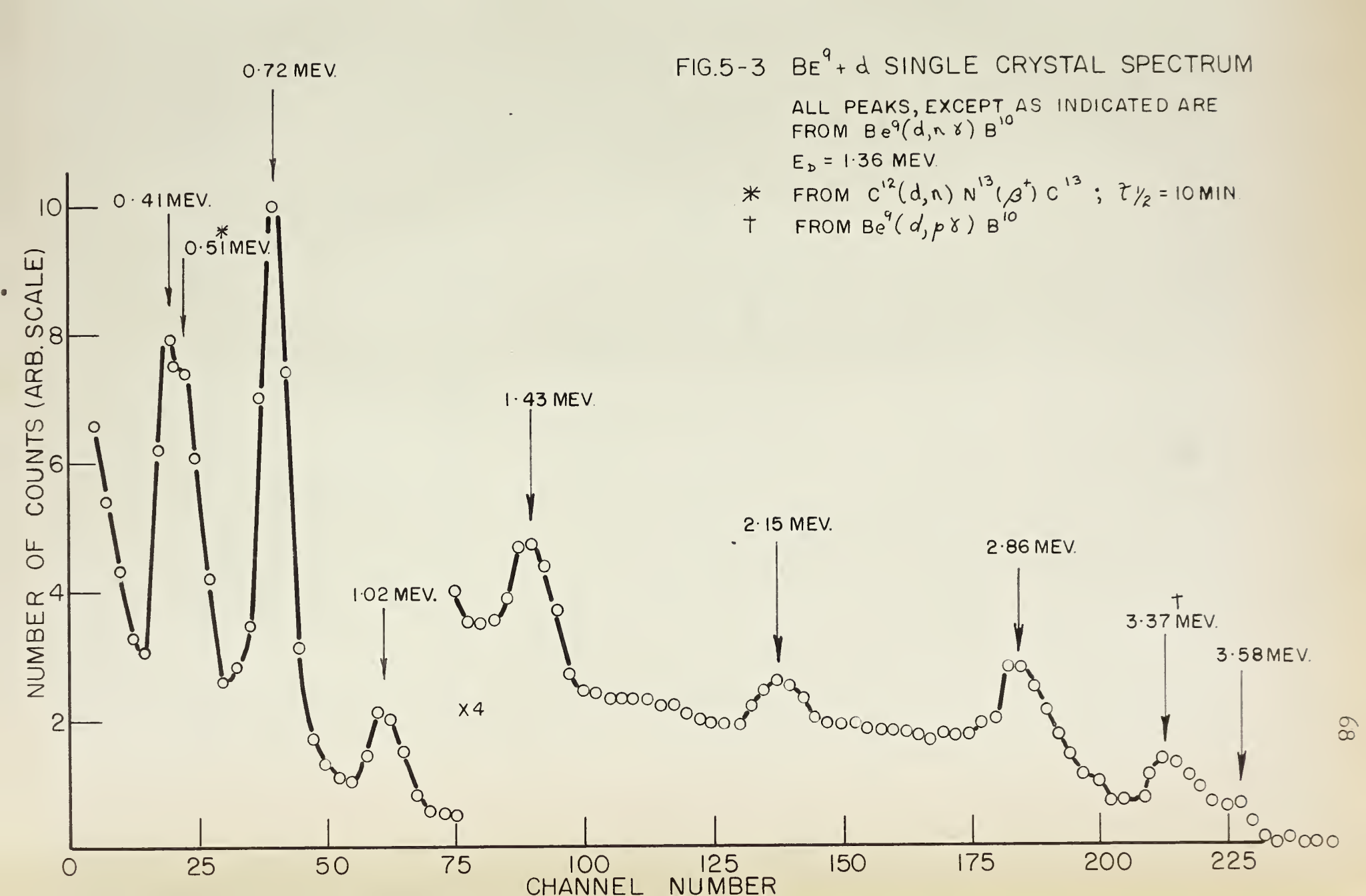
FIG.5-3 $Be^9 + d$ SINGLE CRYSTAL SPECTRUM
ALL PEAKS, EXCEPT AS INDICATED ARE FROM $Be^9(d,n\gamma)B^{10}$
$E_D$ = 1·36 MEV.
* FROM $C^{12}(d,n)N^{13}(\beta^+)C^{13}$ ; $T_{1/2}$ = 10 MIN.
† FROM $Be^9(d,p\gamma)B^{10}$
0·72 MEV.
0·41 MEV.
0·51 MEV.
1·43 MEV.
1·02 MEV.
2·15 MEV.
2·86 MEV.
3·37 MEV.
3·58 MEV.
X4
NUMBER OF COUNTS (ARB. SCALE)
CHANNEL NUMBER
0
25
50
75
100
125
150
175
200
225
2
4
6
8
10

This cascade, the $2.15 \rightarrow 0.72 \rightarrow 0$ cascade, accounts for 40% of the de-excitation (Aj59)* and is the only part of the de-excitation which can be seen by the spectrometer.

In the remainder of this section, cascade intensities taken from Aj59 will be quoted in brackets after the cascade mentioned.

3.58 Mev. level: Of the five possible decay routes, only two are seen by the spectrometer: the $3.58 \rightarrow 0.72 \rightarrow 0$ cascade (60%) and the $3.58 \rightarrow 2.15 \rightarrow 0$ cascade (6%). Figure 5-5 shows the Hoogenboom spectrum of this level from which the branching ratio between the two cascades can be measured. The measured branching ratio is $10.3 \pm 1.5$ to 1, the assigned error being a measure of statistical uncertainty. This figure is in good agreement with the value of 10 to 1 (i.e. 60/6 to 1) obtained using the figures in Aj59. The branching ratio is independent of deuteron energy in the range over which it was measured: 800 to 1800 kev.

Only the yield from the dominant cascade has been plotted in Figure 5-4.

5.16 Mev. level: The 3.58 Mev. level is the last bound state of $B^{10}$. The 4.77 and 5.11 Mev. levels both decay strongly to $Li^6 + \alpha$ so that the gamma-ray yield is too

*Aj59 compiles and summarizes the results of all workers in the field. References to the original papers may be found therein.

small to be accurately measured. The 5.16 Mev. level, however, appears to decay only weakly by alpha-particle emission and is assigned an isotopic spin of one on this basis (Ne58). Two of the five modes of gamma-ray decay can be seen with the spectrometer: the $5.16 \longrightarrow 0.72 \longrightarrow 0$ cascade (29%) and the $5.16 \longrightarrow 2.15 \longrightarrow 0$ cascade (19%). The branching ratio between these two cascades was measured for a deuteron energy of 1800 kev. and is $1.1 \pm .5$ to 1 in fair agreement with the value of 1.5 to 1 (i.e. 29/19 to 1) obtained using the figures in Aj59.

Despite the enhanced gamma-ray yield, it was impossible to obtain a meaningful yield curve in a reasonable length of time.

Each of the three cascades whose yield has been measured proceeds through the 0.72 Mev. level. Since the 0.72 Mev. photopeak was always the best-defined on the experimental spectra, the yield curves are based on the number of counts within it. Before being plotted, this number was corrected for chance coincidences, determined experimentally by inserting 50 mμs. of delay in one channel of the fast coincidence circuit and Compton smear coincidences, using the method outlined in Section 3-4. A Compton coincidence correction was not necessary for the 3.58 Mev. level because of the very small yield from higher energy levels.

FIG. 5–4
YIELD CURVE OF CASCADING GAMMA RAYS FROM $B^{10}$

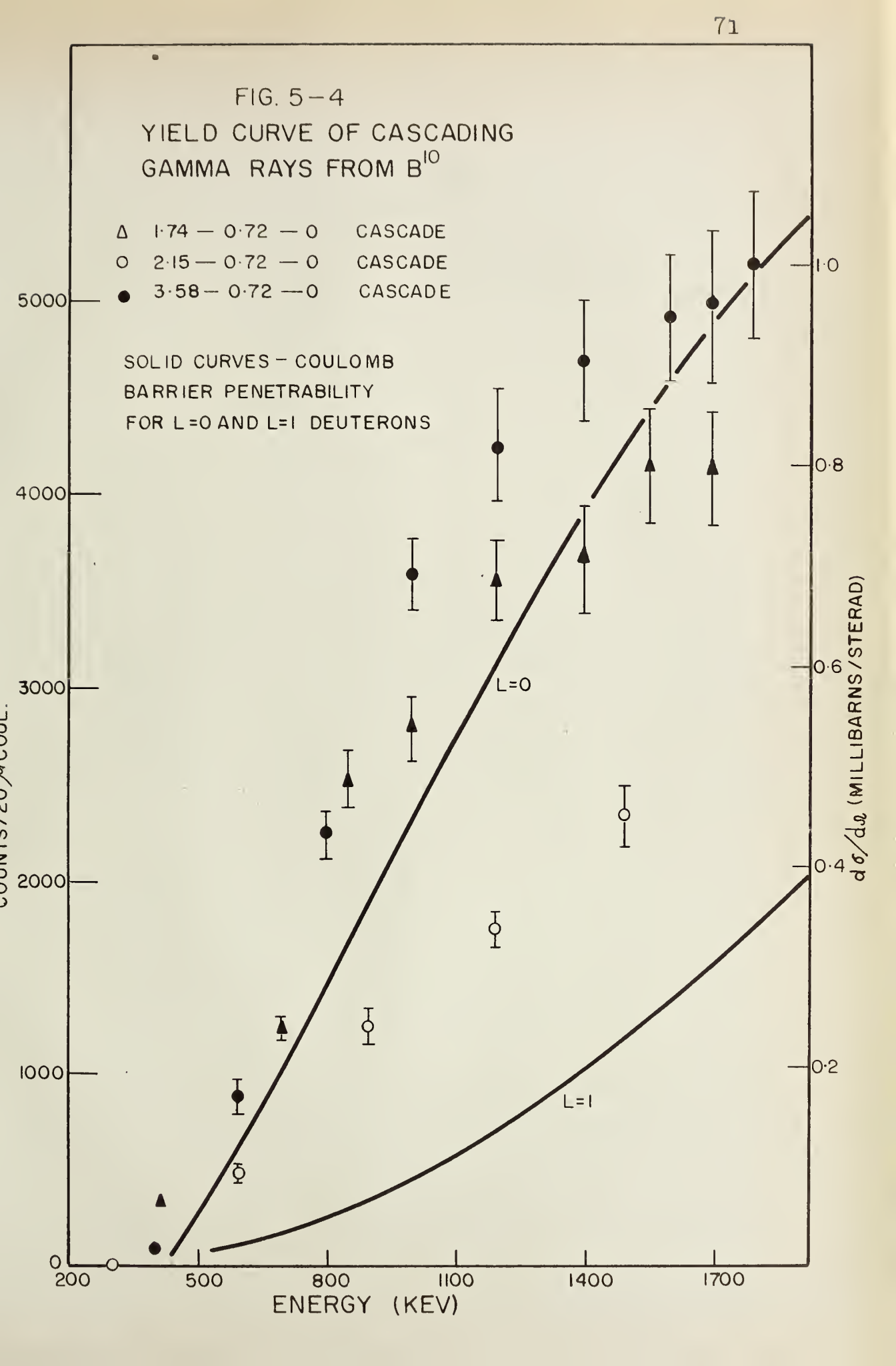

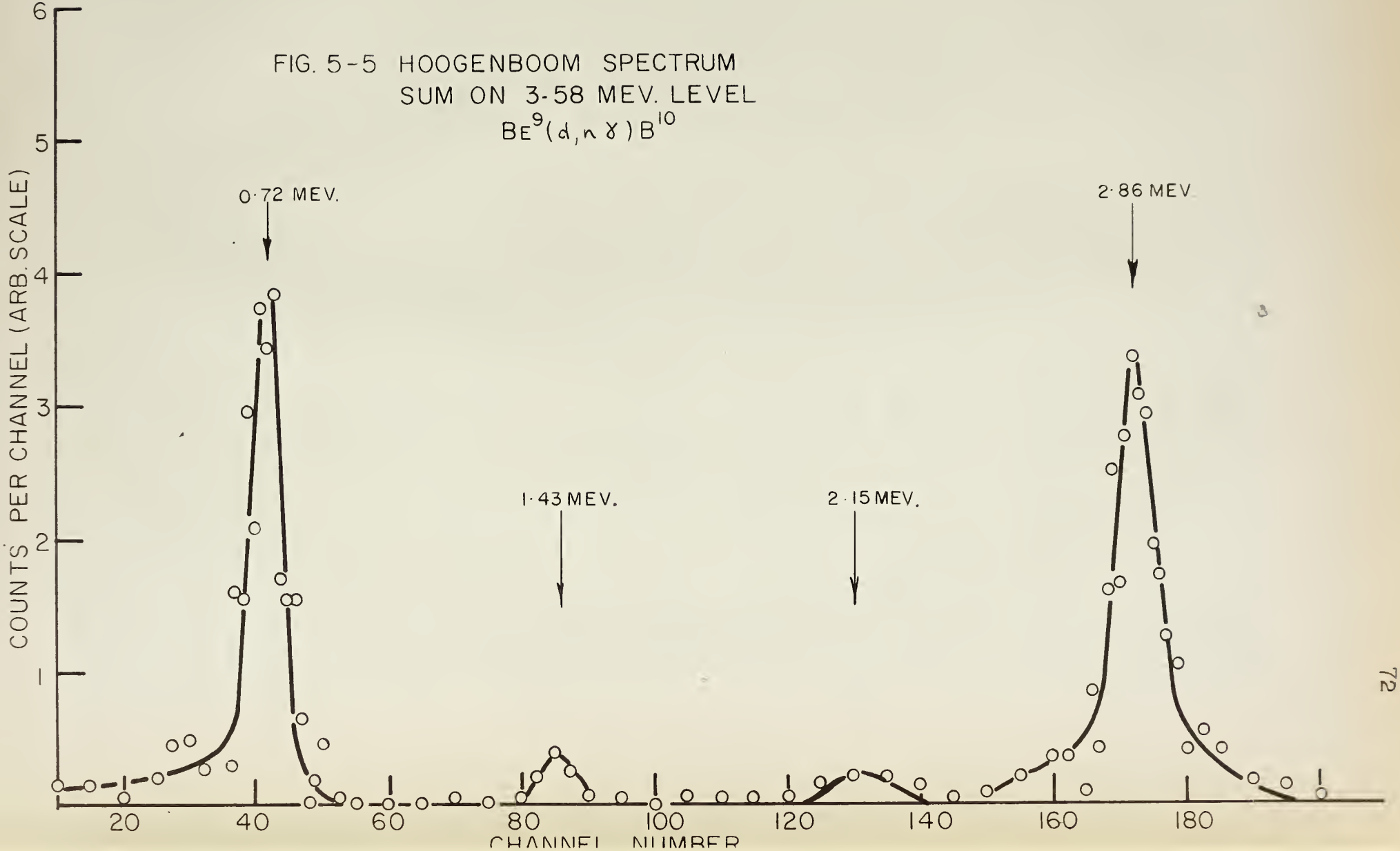
FIG. 5-5 HOOGENBOOM SPECTRUM
SUM ON 3-58 MEV. LEVEL
$Be^9(d,n\gamma)B^{10}$
0·72 MEV.
1·43 MEV.
2·15 MEV.
2·86 MEV.
COUNTS PER CHANNEL (ARB. SCALE)
CHANNEL NUMBER
6
5
4
3
2
1
20
40
60
80
100
120
140
160
180

The curves of Figure 5-4 have also been corrected for efficiency, using the curves of Figures 3-2 and 3-3 in conjunction with the formula for the efficiency of a Hoogenboom spectrometer. Thus Figure 5-4 represents the total number of 0.72 Mev. gamma rays which enter one crystal in coincidence with the other member of the cascade in the other crystal.

Only statistical errors are shown in Figure 5-4. Errors of only 5% in the measurement of photopeak efficiency, resolution and sum channel window width could scale any given curve up or down by as much as 30%. Errors in curve shape should, however, lie within statistical fluctuations.

It should be emphasized that Figure 5-4 shows only the yield from the particular cascade mentioned. These yields can easily be corrected to give the total yield of the level using the branching ratios of Aj59. However, even when corrected, the gamma-ray yield curves are not directly comparable to neutron yield curves from the same levels since a given level may be populated by gamma-ray decays from a higher level as well as directly by the reaction.

The target used, prepared by evaporating beryllium metal onto a platinum backing, was very uniform. Therefore, approximate cross-section determinations could be made and are indicated on the right-hand scale of Figure

5-4. The cross-section was found in the following way.

Target thickness was measured at the very narrow resonance (4 kev. wide) in the reaction $Be^9(p,\gamma)B^{10}$ occuring for a proton energy of 1084 kev. Gamma-ray de-excitation of the 7.48 Mev. level takes place through a single cascade in which a 6.76 Mev. and a 0.72 Mev. gamma ray are produced. The yield was measured by counting the number of gamma rays as a function of energy for energies near the resonance. To reduce background counts, only gamma rays of energy greater than 2.5 Mev. were accepted. The yield curve obtained, corrected for the remaining background, is shown in Figure 5-6. Since the intrinsic width of the resonance is only 4 kev. and the width of the resonance in Figure 5-6 is 40 kev., this latter figure may be taken as a direct measure of the target thickness. Referring to Figure 14-8, Le59, which shows energy loss vs. kinetic energy for protons in various media, it is seen that a 1100 kev. proton loses about 160 Mev. $cm^2/gm$ or 160 x 2.70 = 433 Mev./cm in aluminum (density of aluminum = 2.70 $gm/cm^3$). To a good approximation, only the absorber density affects the rate of energy loss. Thus in beryllium we again have that a 1100 kev. proton loses energy approximately at the rate 160 Mev. $cm^2/gm$ or 160 x 1.85 - 296 Mev./cm (density of beryllium - 1.85 $gm/cm^3$). Therefore the thickness of the

FIG. 5-6 YIELD CURVE $Be^9(p,\gamma)B^{10}$
OVER $E_p$ = 1084 KEV. RESONANCE
($\Gamma_{LAB}$ = 3.8 KEV.)
(CORRECTED FOR BACKGROUND)
TARGET THICKNESS = 0.25 MG/CM$^2$

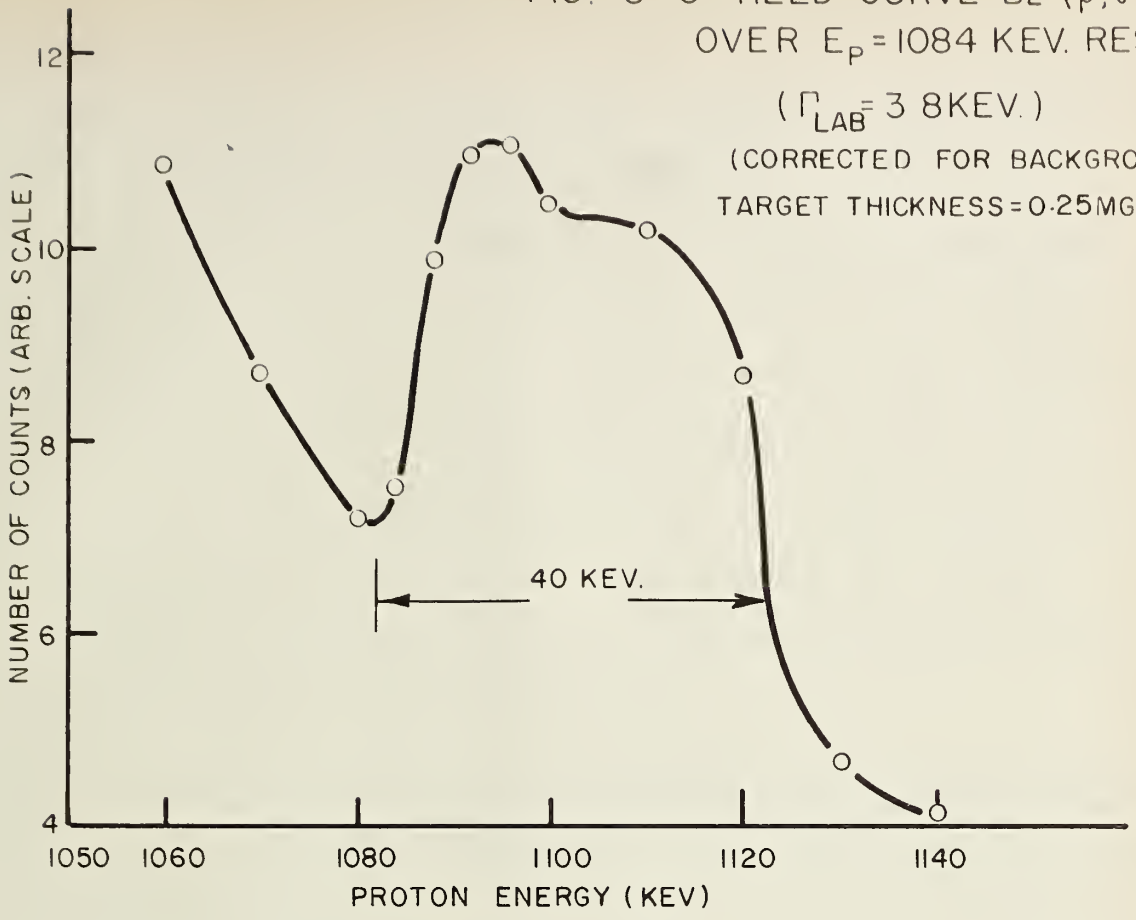


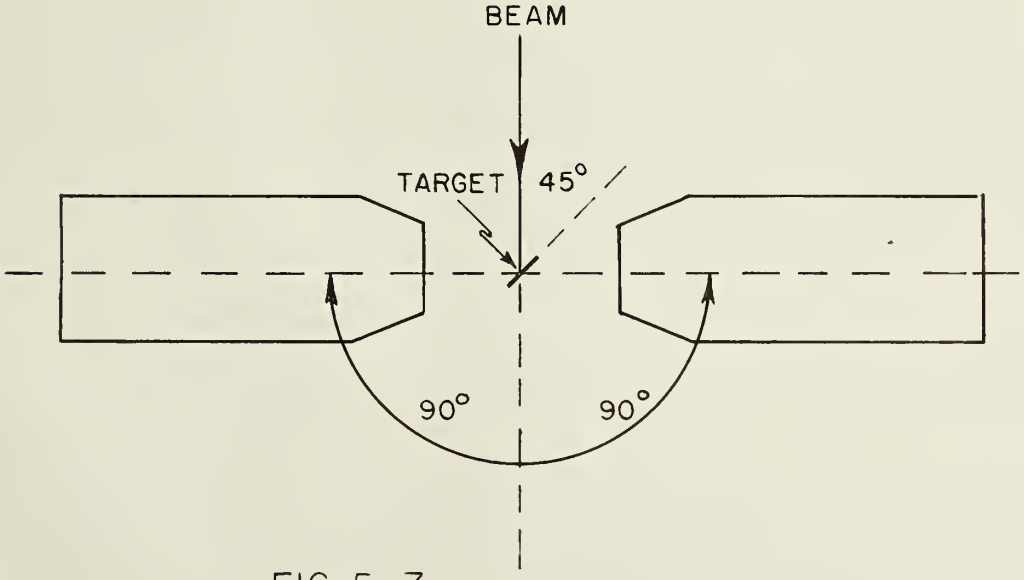


FIG. 5-7
DETECTION GEOMETRY

target is $\frac{40}{160}$ = .25 mg/cm$^2$ (or, dividing by the density, the actual thickness is 1.35 microns).

When the beam is smaller than the target, the cross-section may be defined as the ratio of the total number of events which occur to the product of the total number of incident particles times the number of nuclei per unit area in the target normal to the beam. Thus, if 20 μcoul. of singly-charged particles strike a beryllium target .25 mg/cm$^2$ thick and produce 1000 events of a given kind, the cross-section for the event is

$$\sigma = \frac{1000}{\left(\frac{20\times10^{-6}\ \text{coul.}}{1.60\times10^{-19}\ \text{coul./particle}}\right)\left(\frac{.25\times10^{-3}\ \text{gm/cm}^2\times6.03\times10^{23}\ \text{atoms/mole}}{9\ \text{gm/mole}}\right)}$$

$$= .478\ \mu\text{barns}.$$

Returning again to Figure 5-4, for each count in the 0.72 Mev. peak, there should be a count in the other peak of the cascade. Thus the differential cross-section is given by $d\sigma/d\Omega = .478/4\pi\omega^2$ μbarns/ster./500 counts in 0.72 Mev. peak, where $\omega$ is the solid angle (in spheres) subtended by each detector and has the value $6.3 \times 10^{-3}$ spheres. Substituting, $d\sigma/d\Omega = 96$ μbarns/ster/500 counts in 0.72 peak.

The cross-sections determined are only true for the detection geometry of Figure 5-7 because of possible triple correlation effects. However, a quick check showed

that the triple correlation of the $3.58 \rightarrow 0.72 \rightarrow 0$ cascade is isotropic to within 5% whereas that of the $2.15 \rightarrow 0.72 \rightarrow 0$ cascade has an anisotropy of about 10% at most. The triple correlation of the $1.74 \rightarrow 0.72 \rightarrow 0$ cascade was not examined.

The yield curves found are of some interest because Shpetnyi (Sh57), using photographic plates to observe the neutrons, reports a strong resonance in the reaction rate cross-section in the vicinity of 1 Mev. Since the reaction $Be^9(d,n)B^{10}$ is supposed to take place by stripping, this resonance, if it exists, is very hard to explain. Neilson, Dawson, and Sample (Ne58), using fast neutron time-of-flight techniques, failed to observe it. Figure 5-4 shows that the resonance is not evident in the yield of cascading gamma rays either. Instead, the yield seemed to vary as that of a charged particle penetrating a Coulomb barrier.

The two solid curves of Figure 5-4 give an approximate idea of the Coulomb barrier penetrability for $\ell = 0$ and $\ell = 1$ deuterons. They were calculated using one of several penetration parameters suggested by Freeman and McHale (Fr53) all of which give almost identical results at low energies. The one chosen was $kR/F_L^2+G_L^2$ where $k$ is the propagation constant of the center of mass motion, $R$ is the nuclear radius of $B^{10}$ (found using $R = 1.5 A^{1/3} \times 10^{-13}$ cm),

and $F_L$ and $G_L$ are the regular and irregular Coulomb wave functions. Values of $F_L^2 + G_L^2$ were found from graphs in Sh53.

If the yield curves are divided by the $\ell=0$ penetrability curve (again see Figure 5-4), there appears to be some evidence of a very weak resonance around 1.2 Mev. This possible resonance does not compare with the strong resonance in the yield curve cross-section (uncorrected for penetrability) reported by Sh57. The evidence against this existence of this resonance appears conclusive.

## 5-3. Further Applications of the Spectrometer

The Hoogenboom Spectrometer can only be used to best advantage in measuring the relative amplitude of gamma rays within a prolific cascade. Absolute yield curves are difficult to measure because of many small sources of error whose magnitudes are difficult to determine. On the other hand, experiments such as angular distributions and correlations in which only relative yields are of interest can be performed quite accurately.

The spectrometer is very inefficient and thus high reaction rates (cross-sections of at least 100 μ barns) are desirable to complete an experiment in a time short enough so that any instabilities in the electronics are

not too serious (nor is anybody prepared to start an experiment which is going to take five years to produce a significant number of counts, even if his electronics were completely stable!). The high reaction rate requirement virtually eliminates the study of gamma rays from nuclear levels for which particle emission can also take place and thus eliminates almost all proton-induced reactions. Considerable time was spent studying $Be^{9} + p$ and $B^{11} + p$ reactions but with no success.

Deuteron-induced reactions appear to best meet the high gamma-ray yield requirements. Such reactions do have one disadvantage, although not a very serious one. Neutrons produced in the stripping process can interact with the constituents of the NaI crystal. No evidence of neutron interaction with the iodine content of the crystal was found. However, if thermal neutrons are present, 7 Mev. gamma rays will be produced in the reaction $I^{127}(n,\gamma)I^{128}$. Thus scattered neutrons should not be allowed to reach the crystals. High energy neutrons, however, can and do interact with the sodium content of the crystal via the reaction $Na^{23}(n,n'\gamma)Na^{23}$. One very prolific cascade (cross-section in the order of millibarns) produced in this way was found, the $2.08 \rightarrow 0.44 \rightarrow 0$ cascade of $Na^{23}$. Several other cascades are possible depending upon the neutron energy.

A further and more serious difficulty is that deuteron-induced reactions often produce gamma rays so prolifically that gain shifts in the photomultiplier, discussed in Section 4-1, become a problem. The beam current from the Van de Graaff cannot be held steady enough to ensure that the gain shifts remain constant and cannot be reduced to the point where the gain shifts are insignificant without destroying the machine's stability. The only way around the problem is to eliminate the gain shifts themselves. This could perhaps be done by adding a rather complicated feedback system to regulate the H.T. of the photomultipliers. A gamma-ray source sufficiently strong to be observable over the background from the decay scheme being studied would be used to provide a standard amplitude signal from the photomultipliers. If the amplitude of this signal varied, the deviation from the standard value would be used as an error signal to raise or lower the H.T. as required.

In conclusion, the Hoogenboom spectrometer requires a high yield of cascading gamma rays such as is obtained in stripping reactions. Despite all its limitations, this spectrometer is perhaps the most versatile yet designed for studying gamma rays from one nuclear level at a time.

BIBLIOGRAPHY


Aj59 Ajzenberg-Selove and Lauritsen. Energy Levels of Light Nuclei VI, North-Holland.

Be55 Bell, P. R. Beta and Gamma Ray Spectroscopy (Editor--Siegbahn), North-Holland, Ch. 5, Sect. 5.

Bi53 Biedenharn and Rose. Rev. Mod. Phys., 25 (53) 729.

Ev55 Evans, R.D. The Atomic Nucleus, McGraw-Hill, Ch. 25.

Fr53 Freeman and McHale. Phys. Rev., 89 (53) 223.

Fr55 Frauenfelder, H. Beta and Gamma Ray Spectroscopy (Editor--Siegbahn), North-Holland, Ch. 9, Sect. 1.

Ha51 Hayes and Vickers. Phil. Mag., 42 (51) 1387.

Ho58 Hoogenboom, A. M. Nuclear Instruments, 3 (58) 57.

Kl53 Klema and McGowan. Phys. Rev. 91 (53) 616.

Kr60 Krawciw, W. M.Sc. Thesis, University of Alberta (60).

Le59 Leighton, R. B. Principles of Modern Physics, McGraw-Hill 500.

Li61 Litherland and Ferguson. Can. Jour. Phys., 39 (61) 788.

Ne53 Nelms, A. T. NBS Circular 542 (Graphs of Klein-Nishina Formula, etc.).

Ne58 Neilson, Dawson and Sample. Bull. Am. Phys. Soc., Ser. 2, 3 (58) 323.

Ne59 Neilson, Dawson and Johnson. Rev. Sci. Ins. 30 (59) 963.

Ro53 Rose, M. E. Phys. Rev., 91 (53) 610.

Ro57 Rose, M. E. Elementary Theory of Angular Momentum, Wiley

Sh53 Sharp, Gove and Paul. Graphs of Coulomb Functions, TP1-70, Chalk River Report.

Sh57 Shpetnyi, A. I. Soviet Physics JETP, 5 (57) 357.

Wa50 Walter, Huber and Zünti. Helv. Phys. Acta, 23 (50) 697.